Long-Term Assessment of the Reflectivity Biases and Wet-Radome Effect Using Collocated Operational S- and C-Band Dual-Polarization Radars

Jui Le Loh, Wei-Yu Chang, Hsiu-Wei Hsu, Pin-Fang Lin, Pao-Liang Chang, Yung-Lin Teng, and Yu-Chieng Liou

***Abstract*— This study assessed the long-term radar reflectivity (Z) biases of collocated S- and C-band dual-polarization radars. The systematic bias, wet-radome effect (WRE), and attenuation effect were investigated. The algorithm of self-consistency utilizes Z, differential reflectivity (Z_{dr}), and a specific differential phase (K_{dp}) to estimate the systematic bias and WRE of both radars. Eleven years of disdrometer data in northern Taiwan were used to obtain the self-consistency and K_{dp}-based attenuation correction relation coefficients. Subsequently, a series of sensitivity tests were conducted to examine the influence of these coefficients on bias and attenuation corrections. The $K_{dp}(Z, Z_{dr})$ relationship outperformed that of $K_{dp}(Z)$. The $K_{dp}(Z, Z_{dr})$ relationship with seasonal coefficients and systematic bias-corrected Z_{dr} constituted the optimal procedure. The corrected Z of collocated radars was in good agreement, lending further validity to the correction schemes. The results demonstrated that the stable systematic bias values of two radars were −1.89 to −1.14 dB and −2.46 to −1.87 dB. During the WRE period, additional underestimations of Z by nearly 4 and 7 dB were recorded for S- and C-band radars, respectively. The mean value of radar reflectivity near radar (Z_{nr}) was obtained to identify the WRE period. In this study, an innovative quadratic polynomial fitting equation was proposed to investigate the systematic and WRE biases using Z_{nr}. Moreover, a pronounced wind intensity dependency of the WRE could be observed in the quadratic polynomial fitting equation.**

***Index Terms*— Attenuation, radar data quality, self-consistency, wet-radome effect (WRE).**

I. Introduction

TAIWAN is a subtropical island located between the eastern Asian continent and western North Pacific with a climate primarily modulated by the East Asian monsoons [1]–[3]. Taiwan is also prone to natural disasters triggered by heavy precipitation (e.g., East Asian rainy season and typhoons) because of its geographical and environmental characteristics [4]. Hence, the problems of loss of life and property damage as a result of heavy precipitation-induced disasters [5] are major concerns for various government agencies. Therefore, to mitigate these losses, the real-time monitoring of precipitation is crucial. The meteorological radar is the most suitable instrument for monitoring weather systems and estimating the rainfall rate.

Weather radars have become an indispensable instrument worldwide and play an essential role in meteorological and climatological applications [6]. Radar can detect severe local storms and resultant hazards, and provide quantitative precipitation estimation and hydrometeors' identification [7]–[11]. However, numerous factors, such as hardware issues, surrounding terrain clutter, and the attenuation effect [6], [12], impact the radar data quality. Hence, radar data quality is one factor that determines the success of various quantitative applications [13].

For meteorological applications, C-band radars are widely used. C-band radars operate at a higher frequency than S-band radars and, hence, require a smaller antenna and are cheaper than S-band radars in order to get similar performances [14]. However, past studies have reported that the effects of miscalibration, wet antenna radome, and attenuation in precipitation degrade the data quality of C-band radar and reduce the accuracy of rainfall estimation [11], [13], [15]. Vivekanandan *et al.* [16] indicated that a 1-dB bias in reflectivity (Z, dBZ) produced an 18% bias in the Z-rainfall rate (R) relation. The accurate calibration of radar data is essential for obtaining the maximum benefit from utilizing polarimetric variables [13], [16]–[18].

Ryzhkov *et al.* [17] indicated that Z calibration on operational radars can still be challenging after several decades of research into radar meteorology. Z and differential reflectivity (Z_{dr}, dB) must be calibrated to an accuracy of 1 and 0.2 dB, respectively, for practical applications [18]. The measured $Z(Z^m)$ and $Z_{dr}(Z_{dr}^m)$ are mainly affected by the attenuation effect, hardware systematic bias, and wet-radome effect (WRE). The intrinsic Z (Z^{int}) and Z_{dr} (Z_{dr}^{int}) can be obtained as follows:

$$Z^{int} = Z^m + \text{PIA} + Z^{sys} + Z^{WRE} \quad (1)$$

$$Z_{dr}^{int} = Z_{dr}^m + \text{PIDA} + Z_{dr}^{sys} + Z_{dr}^{WRE} \quad (2)$$

Manuscript received June 24, 2021; revised October 14, 2021, November 18, 2021, December 23, 2021, and March 25, 2022; accepted April 14, 2022. Date of publication April 28, 2022; date of current version May 13, 2022. This work was supported by the Ministry of Science and Technology, Taiwan, under Grant MOST 109-2625-M-008-011 and Grant MOST 107-2111-M-008-042-MY3. *(Corresponding author: Wei-Yu Chang.)*

Jui Le Loh, Wei-Yu Chang, Hsiu-Wei Hsu, Yung-Lin Teng, and Yu-Chieng Liou are with the Department of Atmospheric Sciences, National Central University, Taoyuan 32001, Taiwan (e-mail: haidyloh@g.ncu.edu.tw; wychang@g.ncu.edu.tw; fourfork@g.ncu.edu.tw; yunglin835@gmail.com; tyliou@atm.ncu.edu.tw).

Pin-Fang Lin and Pao-Liang Chang are with the Central Weather Bureau, Taipei 100006, Taiwan (e-mail: pflin@cwb.gov.tw; larkdi@cwb.gov.tw).

Digital Object Identifier 10.1109/TGRS.2022.3170609

where sys and WRE represent systematic bias and WRE, respectively. The PIA (PIA $= 2\int_0^r A_h(r)dr$; dB) and PIDA (PIDA $= 2\int_0^r A_{\mathrm{dp}}(r)dr$; dB) are two-way path-integrated attenuation and differential attenuation at range r (km) from the radar, respectively. A_h (dB km^{-1}) and A_{dp} (dB km^{-1}) are specific horizontal attenuation and differential attenuation, respectively.

The corrections for the attenuation effects of Z and Z_{dr} have been studied intensively, especially in relation to C-band radars [19]–[21]. The specific differential phase (K_{dp}, °km^{-1}) has been extensively used for attenuation correction for several reasons; K_{dp} remains unaffected by attenuation and radar power calibration and is less sensitive to the natural variability of the drop size distribution (DSD) [22]. The relationship of $K_{\mathrm{dp}} - A_h$ and $K_{\mathrm{dp}} - A_{\mathrm{dp}}$ is approximately linear [14], [23].

The differential phase shift (Φ_{dp}, °) is twice the sum of K_{dp} over a specified range, PIA, and PIDA that can consequently be estimated by the increments of Φ_{dp} in the precipitation. This Φ_{dp}-based method [14] is described as follows:

$$\mathrm{PIA} = \alpha \times \Delta\Phi_{\mathrm{dp}} \tag{3}$$

$$\mathrm{PIDA} = \beta \times \Delta\Phi_{\mathrm{dp}} \tag{4}$$

where $\Delta\Phi_{\mathrm{dp}}$ is the increments of observed Φ_{dp} and the coefficients of α and β are in dB $(°)^{-1}$ [11], [24]. These coefficients are sensitive to the variability of the DSD, radar wavelength, temperature, season, and precipitation type [22], [23], [25], [26]. For instance, [26] indicated that the coefficients of the $A_h - K_{\mathrm{dp}}(A_{\mathrm{dp}} - K_{\mathrm{dp}})$ relation of the X-band radar vary greatly from 0.14 to 0.34 (0.11 to 0.17) dB $(°)^{-1}$ as a result of temperature changes and different drop deformation models.

In terms of estimating systematic bias, the self-consistency principle among Z, Z_{dr}, and K_{dp} [27] has been demonstrated to be a reliable algorithm [15]–[17], [22], [25]–[28]. Gorgucci and Baldini [28] corrected Z and Z_{dr} of C-band radar over the region centering on Rome, Italy, based on this principle. Chen *et al.* [11] corrected the attenuation and systematic bias of RCWF S-band and National Central University (NCU) C-band polarimetric radar data over northern Taiwan. Attenuation and systematic bias have both been intensively investigated, but studies of the WRE are relatively few. However, Bechini *et al.* [29] reported that the bias introduced by the WRE is nonnegligible.

The radome condition is one of the critical factors that contribute to measurement bias [30], [31]. Most operational weather radar systems are equipped with a radome to protect the pedestal and antenna from the elements, minimize the high wind load, maintain consistent nominal temperatures, and provide environmental protection to ensure safe operations under severe weather conditions [32]–[37]. However, radomes affect radar performance by attenuating the transmitted and received signals, especially when heavy rain falls on atop the radome [35]–[37]. The attenuation added to Z and Z_{dr} depends on the thickness of the water layer on the radome surface [35], [36].

Kurri and Huuskonen [35] reported that a two-way transmission loss of 3 dB was produced by a dirty and unwaxed radome at C-band under a rain intensity of 15 mm hr^{-1}. The WRE induced Z bias reached 7.5 dB from CASA X-band radars [38]. Moreover, Schneebeli *et al.* [39] obtained a WRE bias of almost 20 dB from a polarimetric X-band radar during heavy tropical rainfall in Brazil. The bias from the WRE is affected by the condition of the radome, precipitation type, and wind conditions [29]–[33], [35]–[37], [39]. Bechini *et al.* [29] indicated that the wind can introduce considerable bias in the wet-radome loss as a function of the azimuth angle. Frech [32] determined that the WRE could be particularly heterogeneous under strong wind conditions because of the inequitable wetness of the radome [40]. Although the influence of the WRE is relatively small for frequencies below the S-band [33], [34], [37], its effects must be considered, especially during heavy rainfall.

The development and improvement of radar data quality algorithms are essential to accurately utilize Z and Z_{dr} adequately. This study: 1) developed a robust and analytic procedure for dual-polarization radars through a long-term assessment of Z bias from collocated S- and C-band dual-polarization radars; 2) examined the influencing factors of the self-consistency algorithm; and 3) analyzed the characteristics and influence of the WRE for both radars. The rest of the article is organized as follows. Sections II and III describe the radar data processing and datasets employed in this study. The long-term monitoring of calibration bias and WRE analysis are then presented in Section IV. Section V discusses the pros, cons, and assumptions of self-consistency and the effect of WRE on radar data quality. Finally, Section VI summarizes and concludes this study.

II. Operational Dual-Polarization Radar Data Processing

The data from the collocated Radar Code of Wu-Fenshan (RCWF-Sband) and Radar Code for Maintenance and Development (RCMD-Cband) were investigated and validated in this study. The Tropical Rainfall Measuring Mission Radar Software Library (RSL) and Lidar Radar Open Software Environment (LROSE) were used for converting the raw NEXRAD and Rainbow 5 (RB5) data to radar universal format (UF) format for RCWF-Sband and RCMD-Cband data, respectively. Bias correction schemes were performed for the Z^m and Z^m_{dr} of both radars, as depicted in Fig. 1.

A. Removal of Nonmeteorological Signals

The quality control process to remove noise and nonmeteorological signals is illustrated in part A of Fig. 1. The copolar correlation coefficient (ρ_{hv}) is useful for the removal of nonmeteorological echoes [41]. Generally, the value of the ρ_{hv} in rainfall with similar raindrop sizes is approximately 0.98 to 1 [42] and yields values less than 0.75 to identify nonuniform scatters (e.g., biological scatters, anomalous propagation, sea and ground clutters, and so on) [43].

The nonmeteorological signals of both radars data were removed when ρ_{hv} was less than 0.85. Next, a noise removal procedure based on the standard deviation (STD) of Φ_{dp} ($\sigma_{\Phi_{\mathrm{dp}}}$) of five neighboring gates was applied to both radars. The data of $\sigma_{\Phi_{\mathrm{dp}}} > 20°$ were, thus, eliminated, and the thresholds were theoretically and empirically determined based on [11].

TABLE I

DATA SAMPLING (SEVEN SEASONALITY OF PRECIPITATION TYPES) USED IN THE STUDY. THE COEFFICIENTS OF α [dB $(^\circ)^{-1}$, (3)], β [dB $(^\circ)^{-1}$, (4)], a_1 AND b_1 [$K_{dp}(Z)$, (11)], a_2, b_2, AND c_2 [$K_{dp}(Z, Z_{dr})$, (9)] FOR RCWF-SBAND (S) AND RCMD-CBAND (C) UNDER DIFFERENT SEASONS AND TEMPERATURES IN 2017

Seasonality of precip. types	Periods	Average Temp. (°C)	α ($\times 10^{-2}$)		β ($\times 10^{-3}$)		a_1 ($\times 10^{-5}$)		b_1 ($\times 10^{-1}$)		a_2 ($\times 10^{-5}$)		b_2		c_2 ($\times 10^{-1}$)	
			S	C	S	C	S	C	S	C	S	C	S	C	S	C
All	Jan−Dec	20	1.97	6.64	2.30	7.90	5.52	9.51	8.94	9.17	1.85	2.61	1.01	1.06	-5.76	-6.41
Winter	Jan−Feb	18	2.70	8.43	2.30	6.10	5.12	8.82	9.06	9.29	1.84	2.43	1.01	1.06	-4.94	-5.52
Spring	Mac−Apr	20	2.09	6.93	2.30	7.80	5.76	9.90	8.86	9.09	1.80	2.78	1.01	1.05	-5.73	-6.10
Meiyu	May−Jun	27	1.54	5.43	2.00	7.60	5.54	9.40	8.95	9.21	1.83	2.39	1.01	1.06	-5.84	-6.07
Summer	Jul−Aug	30	1.47	5.07	1.90	6.50	6.37	11.80	8.69	8.83	1.88	3.92	1.01	1.02	-6.39	-7.21
Typhoon	July 28-30	30	1.55	5.07	1.80	6.10	5.51	9.36	8.96	9.21	1.92	2.34	1.00	1.07	-5.83	-6.56
Autumn	Sept−Nov	24	1.89	6.07	2.10	6.30	5.49	9.27	8.96	9.22	1.96	3.23	1.00	1.03	-5.20	-4.65

TABLE II

BRIEF DESCRIPTION OF SIX DIFFERENT SENSITIVITY TESTS BASED ON $K_{dp}(Z)$ AND $K_{dp}(Z, Z_{dr})$ RELATIONSHIPS. THE COEFFICIENTS OF ALL-SEASON AND SEASONS REFER TO THE CONSTANT COEFFICIENTS (α, β, a_1, b_1, a_2, b_2, AND c_2) OF THE DIFFERENT SEASONALITY OF PRECIPITATION TYPES DETAILED IN TABLE I

Names	Self-consistency algorithm		Coefficients		Z_{dr} systematic bias correction (Z_{dr}^{cor})	
	$K_{dp}(Z)$	$K_{dp}(Z, Z_{dr})$	All-season	Seasonal (S)	Excluded	Included
$K_{dp}(Z)$	✗		✗			
$K_{dp}(Z)^S$	✗			✗		
$K_{dp}(Z, Z_{dr})$		✗	✗		✗	
$K_{dp}(Z, Z_{dr})^S$		✗		✗	✗	
$K_{dp}(Z, Z_{dr}^{cor})$		✗	✗			✗
$K_{dp}(Z, Z_{dr}^{cor})^S$		✗		✗		✗

B. Φ_{dp} *Processing*

The values of the Φ_{dp} along the radial beam may be folded if the Φ_{dp} exceeds the maximum values of Φ_{dp}. Hence, an unfolding process of Φ_{dp} is applied to both radars. Φ_{dp} is subsequently subtracted from the initial values ($\Phi_{dp} = 0^\circ$) to obtain $\Delta\Phi_{dp}$ of both radars, which are used for the attenuation correction of the Z^m and Z_{dr}^m.

C. Attenuation Correction Schemes

Generally, the values of Z^m and Z_{dr}^m are underestimated as a result of rain attenuation [24]. Hence, the attenuated measurements of both radars must be corrected before further application or analysis. K_{dp}, A_h, and A_{dp} were calculated from Joss–Waldvogel disdrometer (JWD) data. The coefficients of α and β in (3) and (4) were obtained through linear regression. The α and β values were optimized through analysis of the different potential conditions in terms of seasons, temperatures, and radar wavelengths. Table I presents the coefficients of α and β of the S- and C-band wavelengths used in this study. Note that all-season coefficients were obtained without analyzing the DSD variabilities. The seasonal coefficients, including six different seasonality of precipitation types (winter, spring, meiyu, summer, typhoon, and autumn [3]) and temperatures, were expected to diminish the influence of DSD variabilities on attenuation correction. Finally, Z^m and Z_{dr}^m can be corrected as follows:

$$Z' = Z^m + \text{PIA} \tag{5}$$

$$Z'_{dr} = Z^m_{dr} + \text{PIDA} \tag{6}$$

where Z' and Z'_{dr} are attenuation-corrected Z^m and Z^m_{dr}.

D. Z_{dr} *Systematic Bias Correction Schemes*

As the vertical pointing scan is not available for RCMD-Cband and RCWF-Sband, Z_{dr}^{sys} was estimated through statistical analysis. According to Chen *et al.* [11], Z_{dr}^{sys} can be estimated using the Z_{dr} characteristic of light rain. The mean DSD-simulated Z_{dr} (Z_{dr}^{dsd}) of light rain (15 < DSD-simulated Z < 25 dBZ) computed from 11 years of JWD data [11], [15] acted as a reference. In this study, the corresponding rainfall rates of the DSD of 15 < DSD-simulated Z < 25 dBZ are less than 4 mm hr^{-1}. The values of Z_{dr}^{dsd} were 0.178 and 0.182 dB for RCWF-Sband and RCMD-Cband, respectively. The averaged Z_{dr} of both radars (Z_{dr}^{rad}) was obtained for a light rain field to avoid the ice phase, rain–ice mixture phase, heavy rainfall, and the attenuation effect. The radar data criteria for the Z_{dr}^{rad} were: 1) height < 3.5 km to avoid the ice and rain–ice phase; 2) 15 < Z^m < 25 dBZ for light rain; 3) a $\rho_{hv} > 0.98$ (0.95) for RCWF-Sband (RCMD-Cband) in pure rain; and 4) $\Delta\Phi_{dp} < 15^\circ$ to avoid the attenuation effect. Thereafter, Z_{dr}^{rad} could be compared with the Z_{dr}^{dsd} to derive the Z_{dr}^{sys} of both radars such that

$$Z_{dr}^{sys} = Z_{dr}^{rad} - Z_{dr}^{dsd}. \tag{7}$$

For example, Z_{dr}^{rad} of RCWF-Sband in the winter season was 0.30 dB; thus, Z_{dr}^{sys} could be calculated to be 0.12 dB using (7).

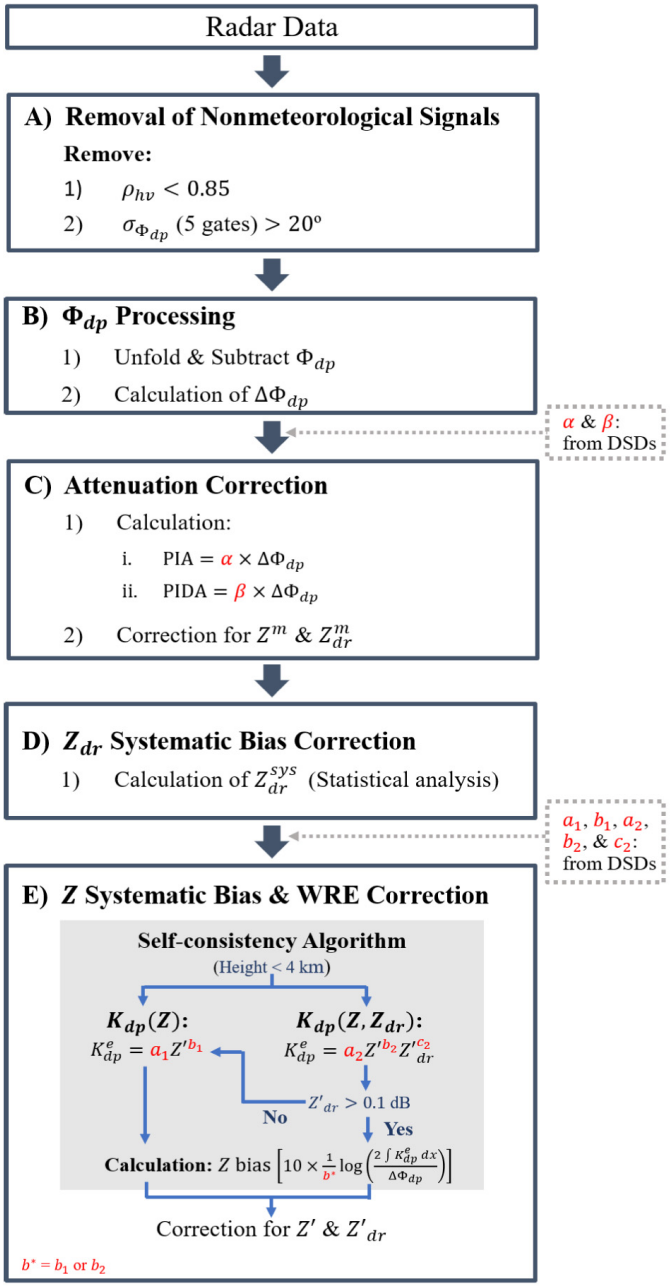

Fig. 1. Flowchart of radar data quality control procedures. The coefficients (α, β, a_1, b_1, a_2, b_2, and c_2) are detailed in Table I. The gray-shaded boxes represent the sensitivity test described in Table II.

E. Z Systematic Bias and WRE Correction Schemes

The last part of the quality control process consisted of the Z bias correction, including the Z^{sys} and Z^{WRE}. Z^{sys} is the systematic bias caused by the radome-induced loss [30], [31], transmit power, and antenna and receiver gain factors [16], [17], [24], [44]. Z^{WRE} is the transmission loss resulting from the wet radome when precipitation falls atop the radar. Z^{WRE} has similar characteristics to the Z^{sys}, and thus, Z bias consisting of both Z^{sys} and Z^{WRE} can be determined using the self-consistency method. No practical algorithm is available for estimating Z^{WRE}_{dr} because of the diverse forms in which the rain accumulates on the radome [11], [30], [31], [33], [36], [37]. Hence, the WRE correction for the Z^m_{dr} was not applied in this study.

According to Vivekanandan *et al.* [16], the Z bias (dB), incorporating Z^{sys} and Z^{WRE}, can be computed using the ratio of the estimated $\Delta\Phi_{dp}$ ($\Delta\Phi^e_{dp}$) and $\Delta\Phi_{dp}$ as follows:

$$Z \text{ bias} = Z^{sys} + Z^{WRE} = 10 \times \frac{1}{b^*} \log\left(\frac{\Delta\Phi^e_{dp}}{\Delta\Phi_{dp}}\right) \tag{8}$$

where the b^* coefficient is either b_1 or b_2, as described in Table I. $\Delta\Phi^e_{dp}$ was derived by integrating the estimated K_{dp} (K^e_{dp}, ° km^{-1}) obtained from the self-consistency algorithm of each radar bin. The calculation of K^e_{dp} was restricted to a height of less than 4 km to eliminate contamination from the melting layer and nonrain hydrometers. The self-consistency algorithm utilizing the Z, Z_{dr}, and K_{dp} measurements, namely, the $K_{dp}(Z, Z_{dr})$, was applied in this study.

K^e_{dp} can be obtained as follows:

$$K^e_{dp} = a_2 Z'^{b_2} Z'^{c_2}_{dr} \tag{9}$$

where Z' is in mm^6 m^{-3} and Z'_{dr} is in linear units. The coefficients of a_2, b_2, and c_2 were obtained using nonlinear least-squares fitting with the Levenberg–Marquardt optimization [11] based on 11 years of JWD data (see Table I). K^e_{dp} of each radar bin was then integrated along a radial to derive the $\Delta\Phi^e_{dp}$, expressed as

$$\Delta\Phi^e_{dp} = 2\int K^e_{dp}\, dr = 2\int \left(a_2 Z'^{b_2} Z'^{c_2}_{dr}\right) dr \tag{10}$$

where dr is the radial resolution of the radar data [16].

The measurement of Z^m_{dr} can be noisy because of nonuniform beam filling, a low signal-to-noise ratio, and so on [24], [45]. The systematic bias and the attenuation correction of Z^m_{dr} have always been challenging when utilizing the operational polarization radar [17]. To avoid applying the noisy values of Z'_{dr} and generating unrealistic values for $\Delta\Phi^e_{dp}$ in (10), (9) is only applied to the data with $Z'_{dr} >$ 0.1 dB. The self-consistency algorithm among the Z and K_{dp} measurements only, namely, $K_{dp}(Z)$, is subsequently applied to the data with a $Z'_{dr} < 0.1$ dB. The calculation of the K^e_{dp} and $\Delta\Phi^e_{dp}$ is done with a similar approach

$$K^e_{dp} = a_1 Z'^{b_1} \tag{11}$$

$$\Delta\Phi^e_{dp} = 2\int K^e_{dp}\, dr = 2\int \left(a_1 Z'^{b_1}\right) dr. \tag{12}$$

The coefficients of a_1 and b_1 were calculated using a linear least-squares fit and are presented in Table I.

F. Sensitivity of the Self-Consistency Algorithm to the DSD Variability and Z_{dr}

Deriving the Z bias from the self-consistency algorithm was mainly influenced by inaccurate coefficients and Z_{dr}. The coefficient values of the self-consistency algorithm were modulated by the DSD [46] although the DSD variations limited the accuracy of the Z calibration [17]. The DSD variability induced an approximate error of 1 dB in the Z calibration [17]. The DSD of northern Taiwan exhibits distinct seasonal variation as a result of its various precipitation

systems [3]. Hence, both the $K_{\mathrm{dp}}(Z)$ and $K_{\mathrm{dp}}(Z, Z_{\mathrm{dr}})$ relationships were obtained for six different seasonality of precipitation types, namely, winter, spring, meiyu, summer, typhoon, and autumn. The calculations of the coefficient were based on DSD measurements and the temperature, as detailed in Table I. Additional coefficients, including all DSD data, were obtained for comparison (indicated as "all-season" in Table II). The influence of the Z_{dr} accuracy on the self-consistency algorithm was also examined. Z_{dr} was discarded in the self-consistency algorithm [using (11) and (12)] to analyze the benefit of including the Z_{dr} measurement. In addition, the effect of the Z_{dr} systematic bias correction on the self-consistency algorithm was also investigated.

The design of the sensitivity test was summarized in Table II. The purpose was to investigate the influence of DSD variability and Z_{dr} systematic bias correction on the Z bias estimation using the self-consistency algorithm. The all-season [$K_{\mathrm{dp}}(Z)$, $K_{\mathrm{dp}}(Z, Z_{\mathrm{dr}})$, and $K_{\mathrm{dp}}(Z, Z_{\mathrm{dr}}^{\mathrm{cor}})$] and seasonal [$K_{\mathrm{dp}}(Z)^S$, $K_{\mathrm{dp}}(Z, Z_{\mathrm{dr}})^S$, and $K_{\mathrm{dp}}(Z, Z_{\mathrm{dr}}^{\mathrm{cor}})^S$] coefficients were applied to the self-consistency algorithm. The sensitivity analysis of the Z_{dr} to the self-consistency algorithm was examined by excluding [(11) and (12)] and including Z_{dr} [(9) and (10)]. The influence of the $Z_{\mathrm{dr}}^{\mathrm{sys}}$ correction on Z^{sys} estimation was also examined by excluding and including $Z_{\mathrm{dr}}^{\mathrm{cor}}$, as presented in Table II. A total of six sensitivity experiments were conducted to examine the influence of the DSD variability and Z_{dr} on the self-consistency algorithm.

G. Comparison of the Calibration Approach

A total of 940 near-synchronized volume scans (within a difference of less than 60 s) from collocated radars were selected for comparison. A set of performance indicators were examined to measure the quantitative performance of the quality control in this study, including the mean difference (MD), STD, the root mean square error (RMSE), and Pearson's correlation coefficient (CORR) as follows:

$$\mathrm{MD} = \frac{1}{N}\sum_{j=1}^{N}\left(Z^{\mathrm{Cband}} - Z^{\mathrm{Sband}}\right)_j \tag{13}$$

$$\mathrm{STD} = \sqrt{\frac{1}{N-1}\sum_{j=1}^{N}\left|\left(Z^{\mathrm{Cband}} - Z^{\mathrm{Sband}}\right)_j - \mathrm{MD}\right|^2} \tag{14}$$

$$\mathrm{RMSE} = \sqrt{\frac{\sum_{j=1}^{N}\left(Z^{\mathrm{Cband}} - Z^{\mathrm{Sband}}\right)_j^2}{N}} \tag{15}$$

$$\mathrm{CORR} = \frac{\sum_{j=1}^{N}\left(\frac{\overline{Z_j^{\mathrm{Cband}} - \mu_{Z^{\mathrm{Cband}}}}}{\sigma_{Z^{\mathrm{Cband}}}}\right)\left(\frac{Z_j^{\mathrm{Sband}} - \mu_{Z^{\mathrm{Sband}}}}{\sigma_{Z^{\mathrm{Sband}}}}\right)}{N-1} \tag{16}$$

where Z^{Cband} and Z^{Sband} are RCMD-Cband and RCWF-Sband, respectively. The MD in (14) is from (13), and $\mu_{Z^{\mathrm{Cband}}}$ ($\mu_{Z^{\mathrm{Sband}}}$) and $\sigma_{Z^{\mathrm{Cband}}}$ ($\sigma_{Z^{\mathrm{Sband}}}$) are the mean and STD of RCMD-Cband (RCWF-Sband), respectively.

H. Wind Retrieval Method: Gradient Velocity Azimuth Display Technique

In this study, the gradient velocity azimuth display (GVAD; [47], [48]) technique was applied to retrieve the wind speed. The GVAD is a modified technique of the velocity azimuth display (VAD), which uses the azimuthal Doppler velocity gradient [49] to estimate the horizontal u and v components (m s^{-1}) atop the radar. The u and v components can be approximated by a Taylor series expansion limited to first derivatives as follows:

$$\begin{aligned} u &= u_0 + \frac{\partial u}{\partial x}x + \frac{\partial u}{\partial y}y \\ v &= v_0 + \frac{\partial v}{\partial x}x + \frac{\partial v}{\partial y}y \end{aligned} \tag{17}$$

where u_0 and v_0 denote the velocity value at the center of the circle being scanned, and x and y refer to the coordinates of a data point [48]. The radial Doppler velocity (V_r) is the component of the wind velocity along the radar radial direction and can be written as

$$V_r = u\cos\theta\sin\phi + v\cos\theta\cos\phi + (w - w_t)\sin\theta \tag{18}$$

where w is the total vertical wind component, w_t is the terminal fall velocity of scattering targets, θ is the elevation angle, and ϕ is the azimuthal angle [48]. The mean u and v above the radar can be determined using a least-squares method with a Fourier expansion on the azimuthal gradients of V_r [48], [50] as follows:

$$\frac{\partial V_r}{\partial \phi} = \sum_{n=1}^{2} n(b_n\cos n\phi - a_n\sin n\phi) \tag{19}$$

[48], where a_n and b_n can be obtained from the curve fitting. Advantages of this technique include being computationally efficient, easily extended to volume velocity processing, and can be carried out using aliased Doppler velocities directly and free of aliasing errors [47]–[49]. Besides, it is relatively insensitive to systematic errors as a result of velocity ambiguities [48]. However, when applying the GVAD technique, the results are limited in data-sparse regions and poor data quality [48], [49]. Details are available in [47] and [48]. The retrieval wind speed was used for the WRE analysis, as described in Section IV-D.

III. Datasets

The JWD and collocated RCWF-Sband and RCMD-Cband data, as presented in Fig. 2, were used in this study. The JWD data from NCU [see Fig. 2(b)] were collected from 2005 to 2015, and quality-controlled for dead-time effects using the procedure suggested by [51]. The 6-min DSD is then calculated to ensure sufficient raindrop sampling numbers of each DSD [3]. Moreover, the DSD data with R less than 1 mm hr^{-1} were also eliminated in this study. There are a total of 30 126 quality-controlled 6-min DSDs available for analysis. The T-matrix scattering method [52] was applied to 6-min DSDs data, and the S- and C-band radar variables, namely A_h, A_{dp}, $\Delta\Phi_{\mathrm{dp}}$, K_{dp}^e, Z, and Z_{dr}, were computed with the assumption of raindrop axis ratio proposed by [53]. The temperature values of raindrops are summarized in Table I. The retrieval radar variables were used to determine the coefficients of α, β, a_1, b_1, a_2, b_2, and c_2, as described in Section II.

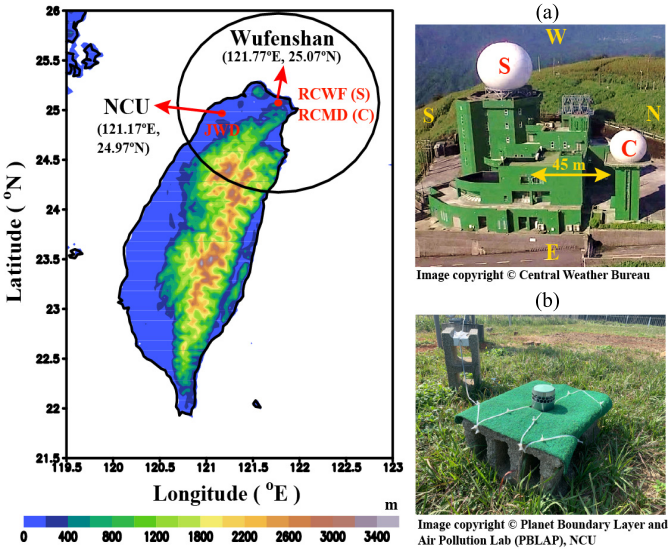

Fig. 2. Geographical locations of collocated operational S- and C-band dual-polarization radars and Joss-Waldvogel disdrometer (JWD), which are located at Wufenshan and National Central University (NCU), respectively, in northern Taiwan. The distance between the radar and JWD is 61 km. Both radars are facing to the east, as shown in (a). The elevation is in meters. (a) RCWF (S) and RCMD (C). (b) JWD.

The collocated RCWF-Sband and RCMD-Cband data in 2017 at Wufenshan [see Fig. 2(a)], operated by the Central Weather Bureau (CWB), were analyzed. The RCWF-Sband data were updated approximately every 6 min, with nine elevation angles (0.5°, 1.5°, 2.4°, 3.4°, 4.3°, 6.0°, 9.9°, 14.6°, and 19.5°). The RCMD-Cband data were updated approximately every 7–8 min with nine elevation angles (0.5°, 1.4°, 2.4°, 3.4°, 4.3°, 6.0°, 9.9°, 14.6°, and 19.5°). Both radars are covered by a spherical sandwich panel radome. The radome of RCMD-Cband is the self-supporting spherical sandwich structure assembled from many panels connected together to form joints. The multilayer sandwich-type with foam core is manufactured with low-loss cores and skins of fiberglass fabric. Similarly, the RCWF-Sband is covered by a foam-core radome with fiberglass where the outer skin is coated with a durable polyurethane semihydrophobic paint to minimize transmission loss. Table III summarizes RCWF-Sband and RCMD-Cband specifications. There are 276 and 202 days with rainy data for RCWF-Sband and RCMD-Cband, respectively.

IV. Results

A. Calibration of Z_{dr}

First, the Z_{dr} bias of RCWF-Sband (RCMD-Cband) was estimated by applying 276 (202) days of data from 2017. The time series of the daily mean Z_{dr}^{rad} from RCWF-Sband and RCMD-Cband is illustrated in Fig. 3, with the vertical bar indicating the STD of the volume mean of Z_{dr}^{rad}. The variations in Z_{dr}^{rad} of both radars were small, especially that of RCWF-Sband [see Fig. 3(a)]. The mean values of Z_{dr}^{rad} varied from 0.12 to 0.33 dB and −0.16 to 0.08 dB for RCWF-Sband and RCMD-Cband, respectively. Z_{dr}^{dsd} (blue dashed line) of light rain was 0.18 dB for both radars. For RCWF-Sband, the Z_{dr}^{rad} (red dashed line) was larger than Z_{dr}^{dsd}, leading to a positive Z_{dr}^{sys} (see Table IV), except in autumn [see Fig. 3(a)]. Conversely, Z_{dr}^{rad} of RCMD-Cband (red dashed line) was smaller than the Z_{dr}^{dsd}, leading to a negative Z_{dr}^{sys} (see Table IV) for all seasons [see Fig. 3(b)]. Z_{dr}^{sys} varied from −0.06 (−0.34) to 0.15 (−0.10) dB for the six seasonality of precipitation types for RCWF-Sband (RCMD-Cband), as presented in Table IV.

TABLE III

Specifications of RCWF-Sband and RCMD-Cband Radar Systems at the Wufenshan Site

Features	Radars	
	RCWF-Sband	RCMD-Cband
Locations		
Longitude (°E)	121.77	
Latitude (°N)	25.07	
Altitude (m)	766	754
Model	NEXRAD WSR-88D	Meteor 1700C
Band and polarimetry	S dual	C dual
Wavelength (cm)	10.5	5.3
Beamwidth (°)	0.93	0.90
Transmitter peak power (kW)	700	250
Radial resolution (m)	250	250
Radome type	Sandwich	Sandwich
Max. radome transmission loss (dB)	0.13	≤0.3
Max. wind loads (km/hr)	324	324
Observation period (min)	∼ 6	∼ 7-8
Scheduled maintenance (days)	7	97

TABLE IV

Z_{dr}^{sys} of Six Different Seasonality of Precipitation Types for RCWF-Sband and RCMD-Cband

Seasonality of precip. types	Z_{dr}^{sys} (dB)	
	RCWF-Sband	RCMD-Cband
Winter	0.12	-0.30
Spring	0.15	-0.21
Meiyu	0.06	-0.10
Summer	0.14	-
Typhoon	0.02	-
Autumn	-0.06	-0.34

B. Calibration of Z

As discussed in Section II-E, the Z bias obtained through the self-consistency method consisted of both Z^{sys} caused by hardware miscalibration and the Z^{WRE} caused by the attenuation of rain on the radome. The mean reflectivity derived from within a radar radius of 10 km, the near-radar Z (hereafter, Z_{nr}), was introduced to define the WRE period. When the value of Z_{nr} was less than the threshold value of 20 dBZ, the calculated Z bias was considered the Z^{sys} only. Additional bias caused by the WRE was noted when the value of the Z_{nr} was greater than 20 dBZ.

An example of Z^{sys} only, free from the WRE, is presented in Fig. 4(a). $\Delta\Phi_{dp}$ and $\Delta\Phi_{dp}^{e}$ of each beam from the RCWF-Sband and RCMD-Cband radars were obtained for the Z^{sys} estimation. In this study, the five farthest consecutive points below freezing level in each beam of $\Delta\Phi_{dp}$ and $\Delta\Phi_{dp}^{e}$ are selected and averaged for the Z bias calculation. To avoid

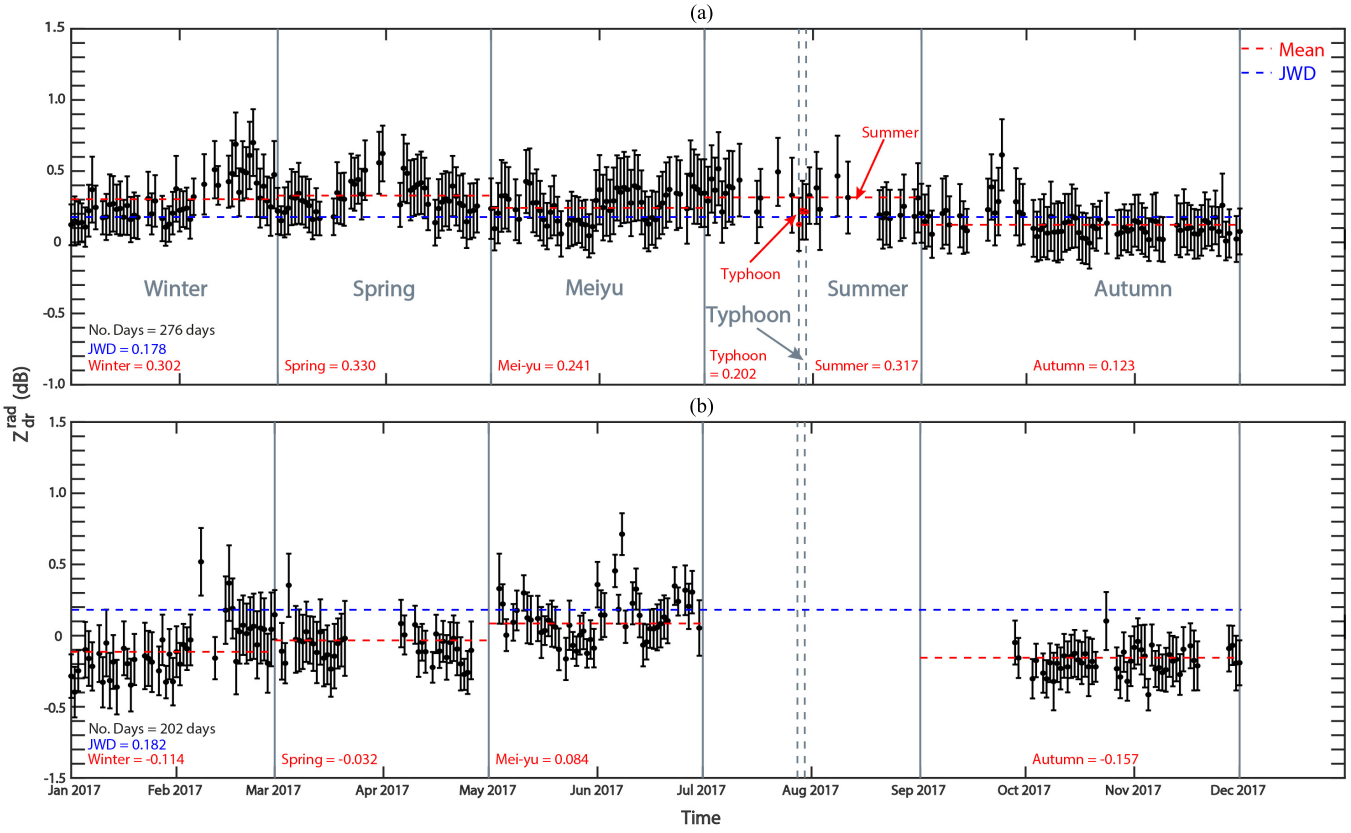

Fig. 3. Temporal variation of daily mean and STD of Z_{dr}^{rad} in 2017 for (a) RCWF-Sband and (b) RCMD-Cband. The blue and red dashed lines represent the values of the Z_{dr}^{dsd} and Z_{dr}^{rad} of each season, respectively. Note that the RCMD-Cband data from July 1 to September 22 were unavailable as a result of scheduled maintenance.

residual attenuation and nonliquid phase precipitation, the RCWF-Sband data are limited to: 1) $5 < \Phi_{dp} < 30°$; 2) elevation angle $< 5°$; and (3) altitude < 4 km for bias calculation. Similarly, for the RCMD-Cband, the Z bias was derived with restrictions of: 1) $5 < \Phi_{dp} < 50°$; 2) elevation angle $< 5°$, and 3) altitude < 4 km. The slopes of the pairs of $\Delta\Phi_{dp}$ and $\Delta\Phi_{dp}^{e}$ were below the nonbiased reference line (solid black line), indicating that the Z measurements of both radars were underestimated. The slopes were, thus, applied to (8) to calculate Z^{sys}. As detailed in Fig. 4(a), the mean Z^{sys} value was -1.29 and -3.18 dB for the RCWF-Sband and the RCMD-Cband, respectively. The WRE introduced additional bias to the Z bias when precipitation fell on the radars, as depicted in Fig. 4(b). Therefore, the overall biases, including Z^{sys} and Z^{WRE}, increased to -2.61 and -6.83 dB for the RCWF-Sband and the RCMD-Cband, respectively, with the additional biases caused by the WRE being approximately 1.32 and 3.65 dB for the RCWF-Sband and the RCMD-Cband, respectively.

Using the self-consistency method, the Z bias, consisting of both the Z^{sys} and Z^{WRE} concurrently, was estimated. Z_{nr} was derived to further assess the precipitation condition on top of the radar site and the influence of the WRE on the Z bias calculation. The data with $Z_{nr} < 60$ (blue bars) and < 20 (red bars) dBZ depicted in Fig. 5 represent heavy and light rain (or no rain) on top of the radome, respectively. The mean (STD) calculated Z bias varied from -1.89 (0.67) to -1.31 (0.79) dB in the six tests of the RCWF-Sband for a $Z_{nr} < 60$ dBZ [see Fig. 5(a)]. However, the mean (STD) Z bias was significantly reduced to 0.20 (0.07) dB for a $Z_{nr} < 20$ dBZ. Similarly, the mean (STD) Z bias of the RCMD-Cband varied from -2.87 (1.45) to -2.43 (1.71) dB for a $Z_{nr} < 60$ dBZ [see Fig. 5(b)]. The mean (STD) Z bias was also reduced to approximately 0.50 (0.30) dB for $Z_{nr} < 20$ dBZ. These results suggested that the WRE introduces additional bias to the reflectivity, increasing the variance of the bias calculation (e.g., a higher STD). Hereafter, Z^{sys} is referred to as the estimated Z bias from $Z_{nr} < 20$ dBZ to avoid the WRE.

As discussed in Section II-F, the influences of DSD variability and Z_{dr} accuracy on the self-consistency algorithm were examined through a series of sensitivity tests. Z^{sys} for six seasonality of precipitation types and sensitivity tests is presented in Fig. 6. Z^{sys} was largely affected by hardware characteristics (e.g., antenna and receiver gains, and transmission) that vary among radars [44]. The Z^{sys} value was expected to remain consistent because of the thorough maintenance of the radar systems by the CWB. Nevertheless, the ranges of the mean Z^{sys} for RCWF-Sband [see Fig. 6(a)] and RCMD-Cband [see Fig. 6(b)] were -2.40 to -0.79 dB and -2.88 to -1.61 dB, respectively. The STD ranges of the Z^{sys} were 0.36 to 0.71 dB and 0.76 to 1.55 dB for RCWF-Sband and RCMD-Cband, respectively; these variations were mainly attributable to the

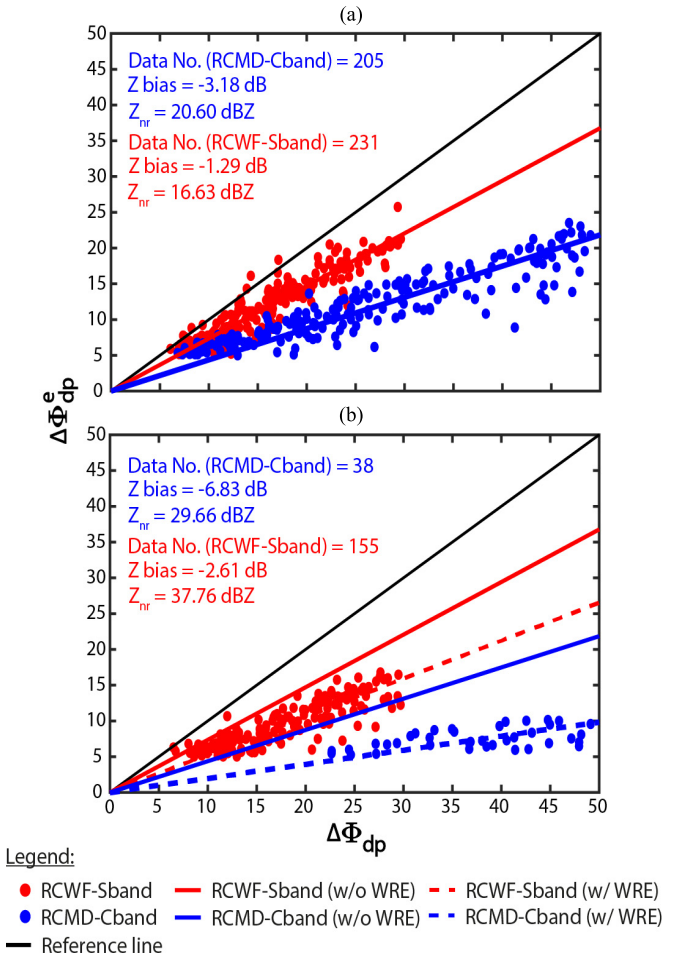

Fig. 4. Scatterplot of $\Delta\Phi_{dp}$ and $\Delta\Phi^{e}_{dp}$ during (a) 0128 (0123) and (b) 0156 (0158) UTC June 2, 2017, from the RCWF-Sband (RCMD-Cband). The red (blue) dotted and solid lines for the RCWF-Sband (RCMD-Cband) indicate the slope of the $\Delta\Phi_{dp}$ and $\Delta\Phi^{e}_{dp}$ derived from (8).

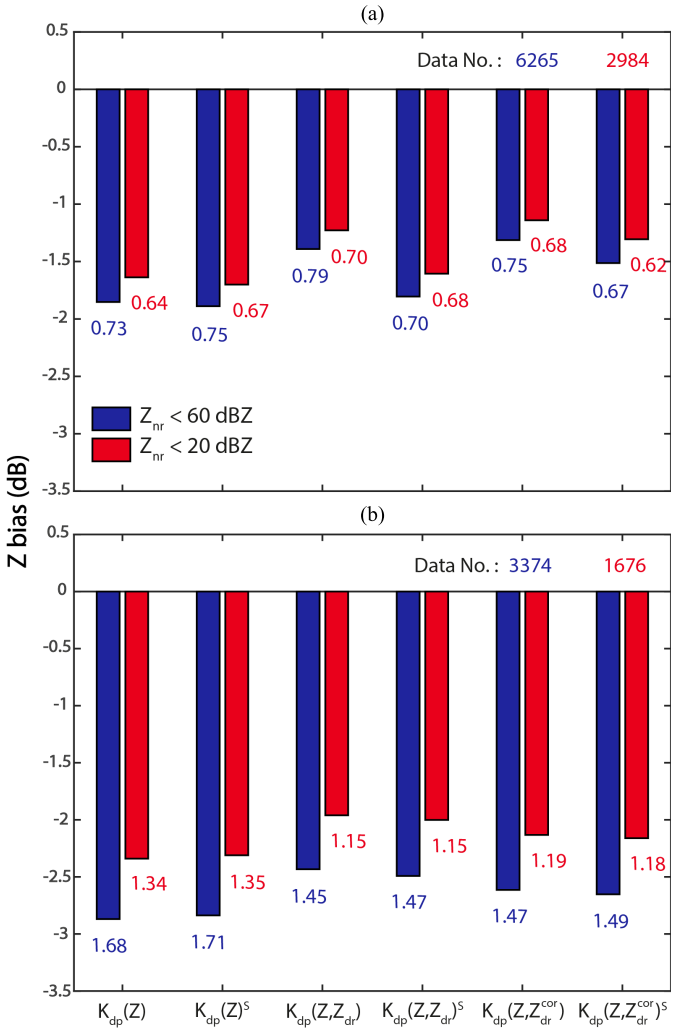

Fig. 5. Comparison of the average Z bias with the Z_{nr} < 60 (blue) and 20 (red) dBZ of six different sensitivity tests (see Table II) in 2017 for (a) RCWF-Sband and (b) RCMD-Cband. The data number in blue (red) represents the total data number for Z_{nr} < 60 (20) dBZ. The number digits represent the values of the STD of the Z bias.

DSD variability. The DSD variability induces the coefficient uncertainties of both the self-consistency algorithm and attenuation correction. In addition, the systematic bias of Z_{dr} was essential for the estimated Z^{sys}.

To determine the optimal procedures for estimating Z^{sys}, the STD values of the Z^{sys} from six sensitivity tests were examined. As illustrated in Fig. 6(c), the $K_{dp}(Z, Z_{dr})$ relations (light and dark green or red bars) have comparable STD values for all seasonality of precipitation types. Notably, $K_{dp}(Z, Z_{dr}^{cor})^{S}$ had the lowest STD of the Z^{sys} [0.62 dB in Figs. 5(a) and 6(c)]. For RCMD-Cband [see Fig. 6(d)], the $K_{dp}(Z, Z_{dr})$ relation also had lower values of STD for the Z bias than the $K_{dp}(Z)$ relation. The STD of Z^{sys} from $K_{dp}(Z, Z_{dr}^{cor})^{S}$ was significantly reduced [1.18 dB in Figs. 5(b) and 6(d)]. In general, both radars could be calibrated well among the six tests, especially for the $K_{dp}(Z, Z_{dr})$ relations. Overall, $K_{dp}(Z, Z_{dr}^{cor})^{S}$ (pink bars) of both radars recorded the lowest STD [see Fig. 6(c) and (d)] and provided the most consistent estimation of Z^{sys}. $K_{dp}(Z, Z_{dr}^{cor})^{S}$ is, thus, considered as the optimal procedure of deriving Z^{sys} and selected for further analysis.

Fig. 7 describes the daily mean and seasonal mean Z^{sys} of RCWF-Sband and RCMD-Cband. It shows that both radars have a fairly consistent daily mean Z^{sys}, but the decreased daily mean Z^{sys} of RCMD-Cband can be noticed in early March and April. This temporarily decreasing was caused by the additional WRE bias, which was not properly removed by a 20-dBZ threshold. Nevertheless, those cases have a minor impact on seasonal mean Z^{sys}. Both radars revealed a consistent seasonal mean Z^{sys} varied from −1.89 to −1.14 dB and −2.46 to −1.87 dB for RCWF-Sband [see Fig. 7(a)] and RCMD-Cband [see Fig. 7(b)], respectively. These uncertainties are mitigated by performing a season running average of the calibration values, but they are still present as seasonal variations in the calibrations. These seasonal variabilities in Z^{sys} were adequately low at approximately 0.75 and 0.59 dB for RCWF-Sband and RCMD-Cband, respectively. Kwon *et al.* [15] also demonstrated bias variation using an S-band dual-polarization radar at Mountain Bisl during a rain event with an approximate variation of 0.5–0.8 dB. This method can achieve an accuracy of 0.5–1 dB for Z calibration.

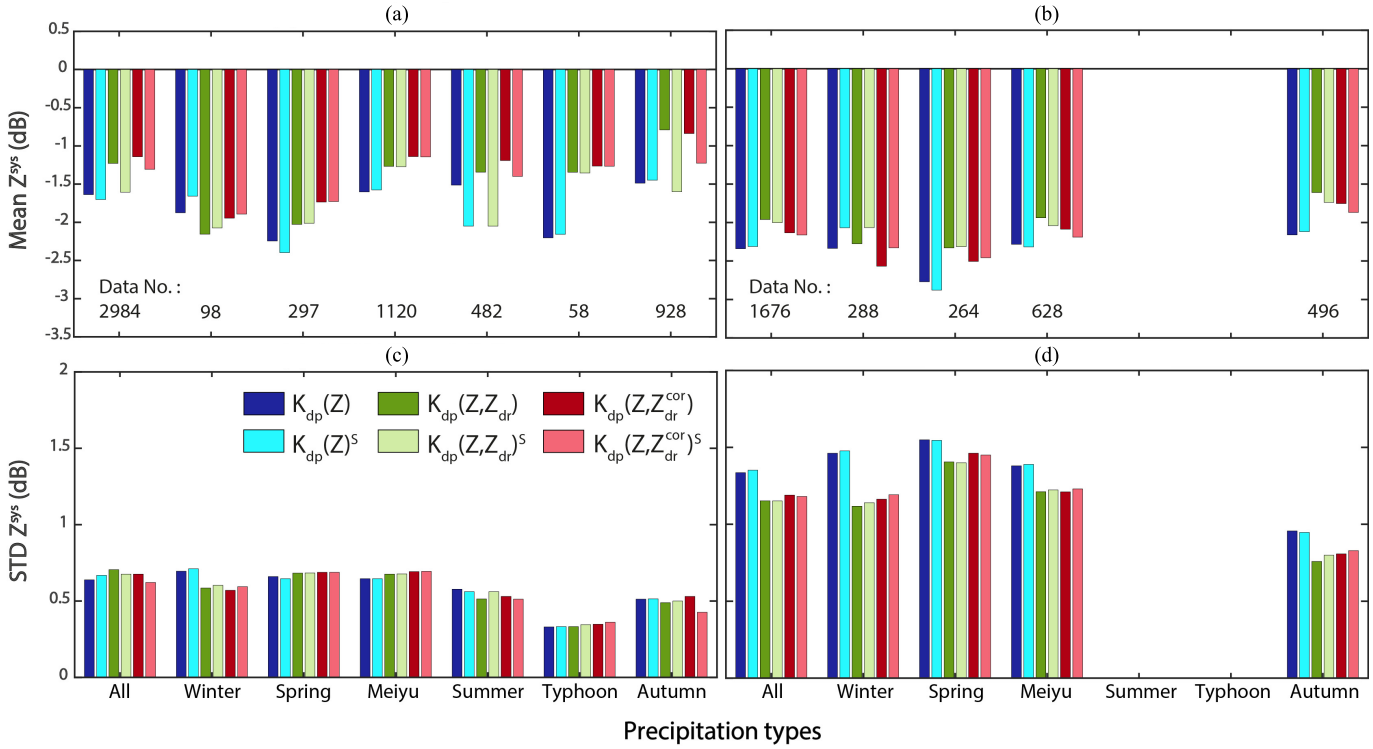

Fig. 6. Same as Fig. 5 but for Z^{sys} ($Z_{nr} < 20$ dBZ) for seven seasonality of precipitation types for (a) and (b) mean and (c) and (d) STD of Z^{sys}.

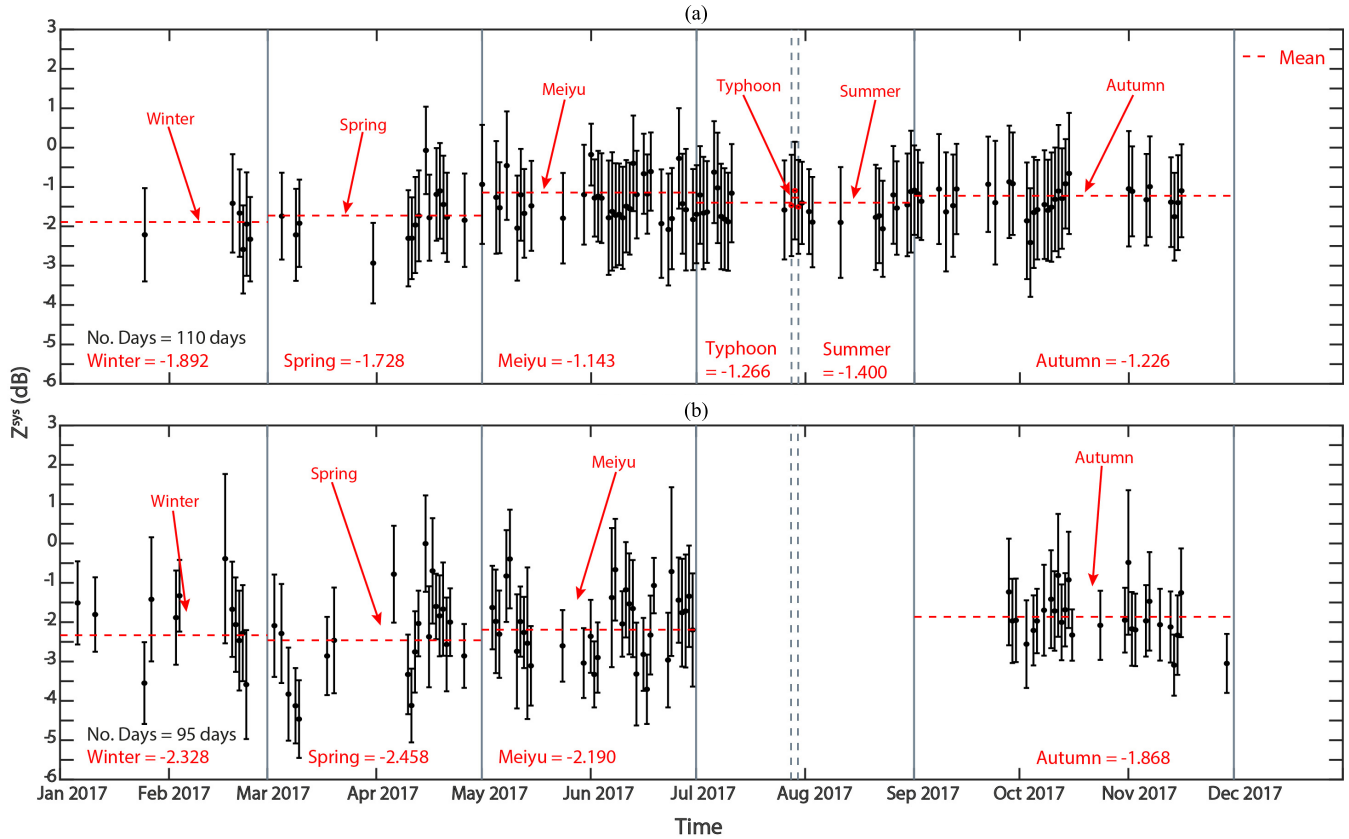

Fig. 7. Same as Fig. 3, but for Z^{sys} of $K_{dp}(Z, Z_{dr}^{cor})^S$ for (a) RCWF-Sband and (b) RCMD-Cband. The red dashed line represents the mean values of Z^{sys} of each season.

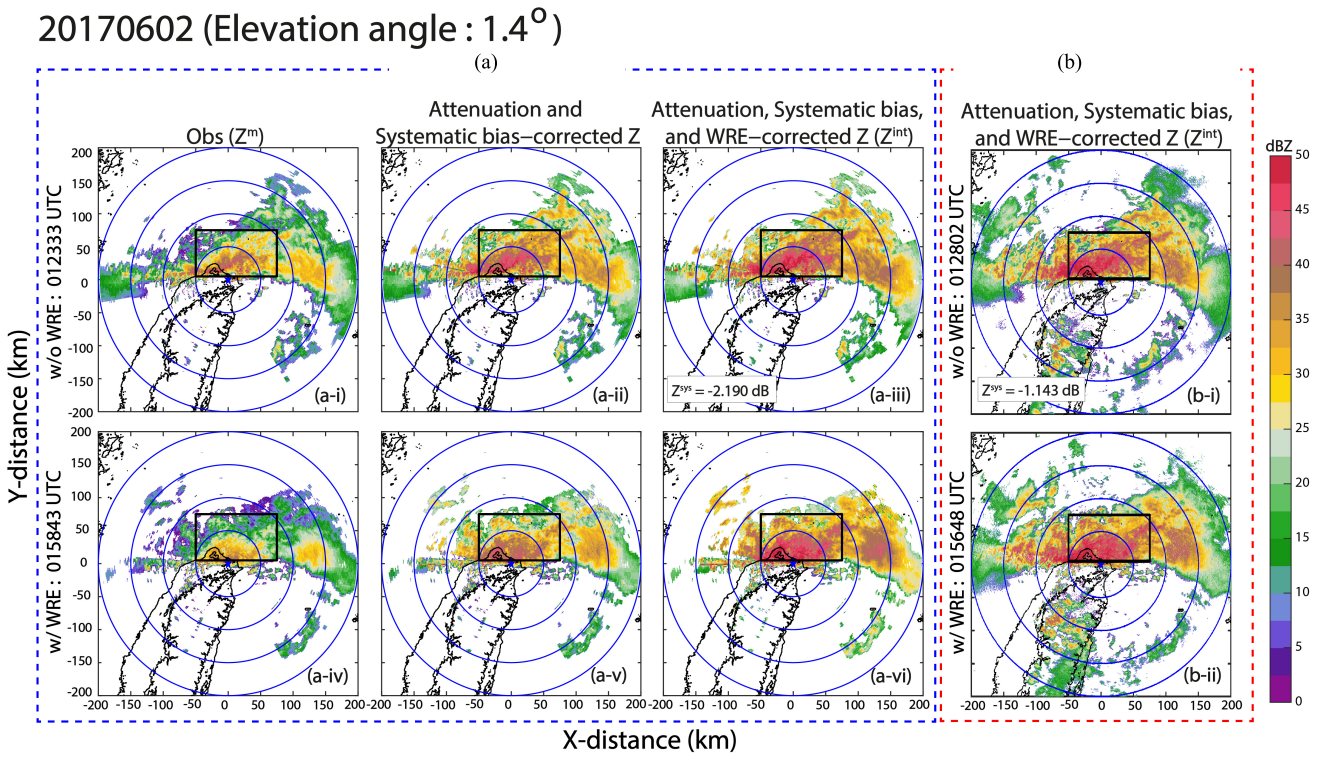

Fig. 8. Plan position indicators images of before (Z^m [a-i and a-iv]) and after the quality control (attenuation and systematic bias−corrected Z [a-ii and a-v] and Z^{int} [a-iii, a-vi, b-i, and b-ii]) of (a) RCMD-Cband (blue dotted square box) and (b) RCWF-Sband (red dotted square box) on June 2, 2017, at elevation angle 1.4°. Comparison between with (0158 [a-iv to a-vi] and 0156 [b-ii] UTC) and without the WRE (0123 [a-i to a-iii] and 0128 [b-i] UTC) for both radars. The blue pentagram represents the location of the radar. The black square box denotes the area enhanced of Z values after all quality control compared with those before quality control.

C. Comparison of RCWF-Sband and RCMD-Cband

The collocation of the RCWF-Sband and RCMD-Cband radars provided a unique opportunity to validate the Z bias. Fig. 8 depicts plan position indicators images of an east–west oriented squall line on June 2, 2017, before (Z^m) and after the quality control (attenuation and systematic bias-corrected Z and Z^{int}) of both radars. The reflectivities from RCWF-Sband (RCMD-Cband) at an elevation angle of 1.4° at 0128 (0123) UTC (without the WRE) and 0156 (0158) UTC (with the WRE) were compared. The seasonal mean Z^{sys} of the meiyu for RCMD-Cband and RCWF-Sband was −2.19 and −1.14 dB, respectively, as presented in Fig. 7 and applied in this selected case (see Fig. 8). The values of Z are enhanced over the entire area after attenuation and systematic bias correction [see Fig. 8(a-ii) and (a-v)], especially in the black square box of Fig. 8. The Z^m values of RCMD-Cband [see Fig. 8(a-i) and (a-iv)] increased significantly to > 45 dBZ [see Fig. 8(a-ii) and (a-v)]. However, systematic lower values for the attenuation and systematic bias-corrected Z were noted at 0158 UTC rather than at 0123 UTC. The squall line was atop the radar at 0158 UTC, suggesting that the WRE introduced additional attenuation because of the rain on the radome. Z^{WRE} of RCMD-Cband [the difference between Fig. 8(a-ii) and (a-v)] was approximately 4 dB. Fig. 8(a-iii) and (a-vi) details the values of the Z^{int}, which were in good agreement with RCWF-Sband [see Fig. 8(b)]. The consistency between the corrected Z of RCMD-Cband and RCWF-Sband further validated the effectiveness of the quality control steps.

The quantitative comparisons before and after quality control procedures for the RCWF-Sband and RCMD-Cband radars are exhibited in Fig. 9, indicating the Z difference between RCMD-Cband and RCWF-Sband ($Z^{\text{Cband–Sband}}$) before and after quality control from the selected meiyu case (June 1 and 2, 2017) at an elevation angle of 1.4°. Fig. 9(a) describes the raw data of $Z^{\text{Cband–Sband}}$, which decreased as $\Delta\Phi_{\text{dp}}$ of RCMD increased as a result of the attenuation effect, systematic bias, and WRE. The values of $Z^{\text{Cband–Sband}}$ markedly improved after all bias corrections [see Fig. 9(b)]. The distribution was, thus, shifted upward and closer to the black dashed line. Nevertheless, the distribution was slightly lower in relation to the black dashed line when $\Delta\Phi_{\text{dp}}$ of RCMD was larger than 150°, which may be attributable to the limitation of the Φ_{dp}-based attenuation correction algorithm. The MD, STD, and RMSE values decreased to -4.40×10^{-3}, 3.15, and 3.15 dB, respectively, and the CORR of all corrected $Z^{\text{Cband–Sband}}$ increased from 0.78 to 0.93 (see Table V).

A set of performance indicators were obtained for both radars on June 1 and 2, 2017, as described in Table V. The observed $Z^{\text{Cband–Sband}}$ had the highest values for MD (−2.98 dB), STD (4.17 dB), and RMSE (5.13 dB) in 2017. The MD, STD, and RMSE decreased to −0.69, 4.07, and 4.13 dB, respectively, following all bias corrections. The CORR of all corrected $Z^{\text{Cband–Sband}}$ of 2017 increased from 0.83 to 0.87. Z^{int} of RCWF-Sband and RCMD-Cband were in good

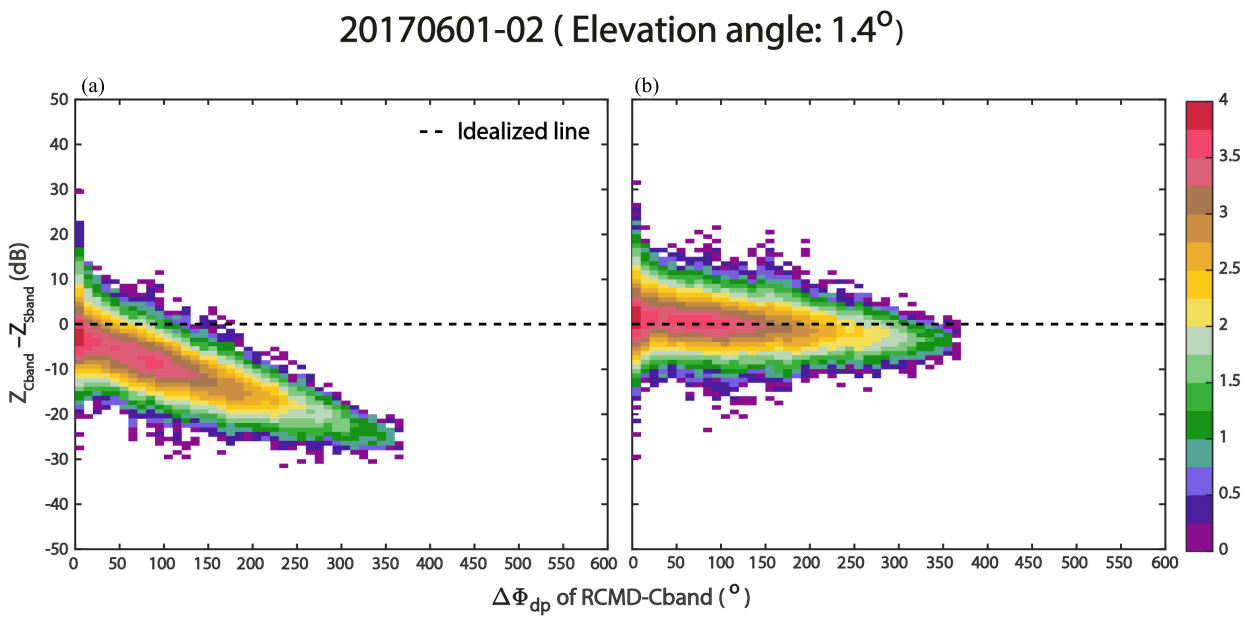

Fig. 9. Comparison of the Z difference of RCMD-Cband and RCWF-Sband within a 60-s time difference for (a) observation and (b) all quality control of the selected meiyu case (June 1 and 2, 2017) at an elevation angle of 1.4°. The black dashed line represents the idealized line ($y = 0$). The colorbar is in logarithmic scale; units are counts.

TABLE V

COMPARISON BETWEEN S- AND C-BAND RADAR STATISTIC METRICS BEFORE AND AFTER CORRECTION FOR SELECTED MEIYU CASE (JUNE 1 AND 2, 2017) AND 2017 AT AN ELEVATION ANGLE OF 1.4°

Statistics	$Z_{Cband} - Z_{Sband}$ Observed		$Z_{Cband} - Z_{Sband}$ All Corrected	
	Meiyu	2017	Meiyu	2017
MD (dB)	−6.85	−2.98	-4.40×10^{-3}	−0.69
STD (dB)	5.10	4.17	3.15	4.07
RMSE (dB)	8.54	5.13	3.15	4.13
CORR	0.78	0.83	0.93	0.87

agreement, lending further validity to the correction schemes. Therefore, $K_{dp}(Z, Z_{dr}^{cor})^S$ can improve data quality by reducing the systematic, WRE, and attenuation biases.

D. WRE Analysis

Other studies reported that the bias introduced by the WRE is nonnegligible, which is further discussed in this section. The quasi-vertical profiles of the Z^m from the meiyu [see Figs. 10(a)–11(a)] and typhoon [see Fig. 12(a)] cases revealed the vertical structure of the precipitation system near the radar. Both meiyu cases recorded heavy rainfall during 19 to 23 UTC on June 1, 2017, and 01 to 05 UTC on June 2, 2017 [see Figs. 10–11(a)]. Fig. 12(a) describes heavy rainfall during 11 to 14 UTC on July 29, 2017.

Figs. 10–12(b) present the time series of the Z_{nr} and Z bias of these cases. Consistent with Fig. 7, the Z bias (solid red line) of both cases exhibited a uniform mean Z^{sys} (red dashed line), slightly higher than the −1.15 dB in the meiyu case of RCWF-Sband [see Fig. 11(b)]. Figs. 10–11(b) indicate that Z was underestimated by almost 6 and 9 dB for the RCWF-Sband and RCMD-Cband radars, respectively; this occurred when Z_{nr} (blue solid line) was higher than 30 dBZ, especially between 02 and 05 UTC on June 2, 2017. However, the typhoon case from the RCWF-Sband radar exhibited an almost uniform Z bias, despite Z_{nr} being higher than 30 dBZ (11–13 UTC on July 29, 2017), as presented in Fig. 12(b). The high wind speed in the typhoon case may be subject to a different WRE, similar to the low wind speed in the meiyu case. To examine the influence of wind speed on the WRE, the calculated Z bias and Z_{nr} were investigated.

Fig. 13 illustrates the relation between wind speed, Z bias, and Z_{nr} for the meiyu and typhoon cases. Both meiyu cases demonstrated that the average Z bias was higher when precipitation was greater atop the radome ($Z_{nr} > 30$ or 40 dBZ) under the low wind speed condition. By contrast, for RCWF-Sband, the Z bias for Z_{nr} values larger and smaller than 40 dBZ in the typhoon cases (black open and closed circles) remained consistent. Therefore, the strong wind speed in the typhoon case may have reduced the WRE by removing the raindrops atop the radome. Notably, the measured wind speed was validated and in good agreement with the observed wind speed from the CWB automatic weather station (not shown). In the following, we analyze the relationships between the Z bias and Z_{nr} under different wind speed conditions.

As described in Fig. 14, the Z bias of RCWF-Sband exhibited a clear downward trend across Z_{nr}, especially when $Z_{nr} > 20$ dBZ. The red and black circles represent the mean Z bias when $Z_{nr} > 40$ dBZ in the meiyu and typhoon cases, respectively. The mean Z bias of the typhoon cases (black circle) had less bias because of the stronger wind speed, as previously discussed. To further investigate the influence of wind speed on the Z bias, the values of the mean Z bias of the $Z_{nr} > 40$ dB were categorized as weak (wind speed $\leq$ 6 ms^{-1}), moderate (6 < wind speed $\leq$ 12 ms^{-1}), and strong

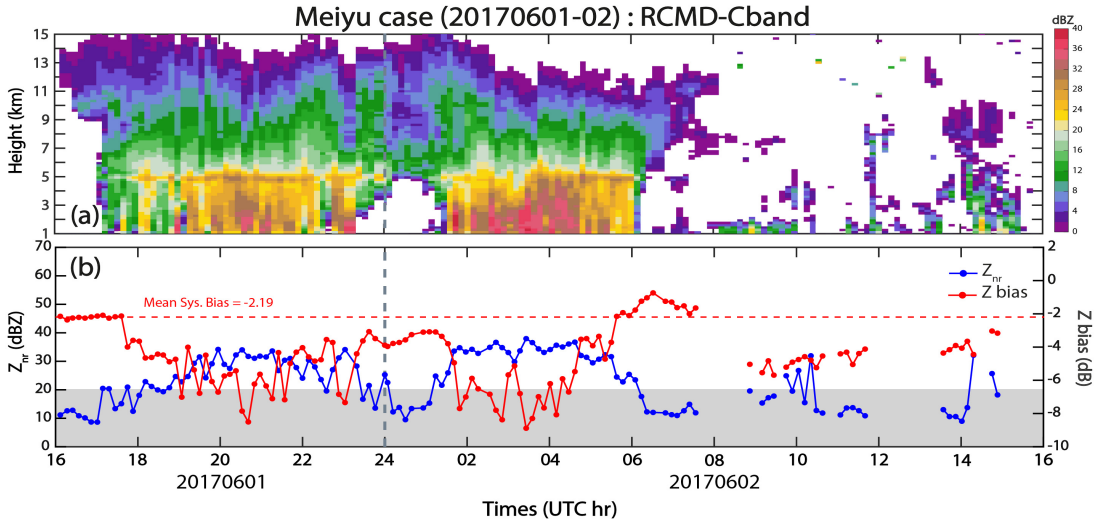

Fig. 10. Time series of (a) quasi-vertical profiles of Z^m at an elevation angle of 19.5° and (b) Z_{nr} (blue) and Z bias (red) for the selected meiyu case (June 1 and 2, 2017) of RCMD-Cband. The red dashed line represents the mean Z^{sys}. The light gray-shaded box represents the area of light rain ($Z_{nr} < 20$ dBZ).

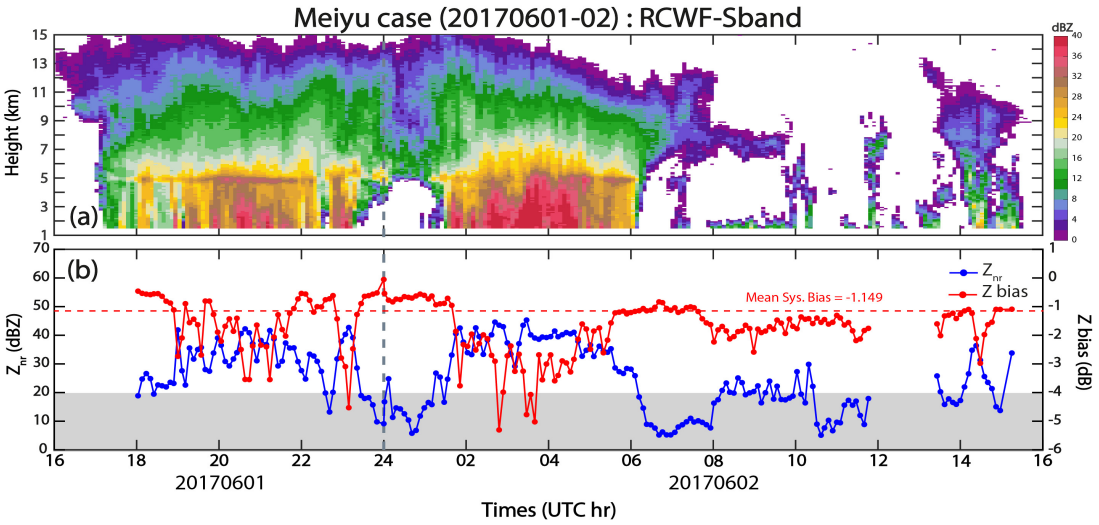

Fig. 11. Same as Fig. 10, but for RCWF-Sband.

(wind speed > 12 ms^{-1}) wind speeds. As illustrated in Fig. 14, the Z bias gradually decreased from weak (pink square, Z bias $= -2.94$ dB) to moderate (gray square, Z bias $= -2.48$ dB) and to strong wind speed (light blue square, Z bias $= -2.05$ dB). Because of the limited available data on wind speed conditions, only two fit quadratic polynomial equations of different wind speeds were proposed (wind speed ≤ 6 ms^{-1} and wind speed > 12 ms^{-1}) for RCWF-Sband. By utilizing these equations, the systematic bias (intercept of the equations) and WRE (red and blue solid curve lines) can simultaneously be derived through the application of Z_{nr} and wind speed. The systematic biases obtained from both equations were -1.31 and -1.37 dB, consistent with the mean Z^{sys} of $K_{dp}(Z, Z_{dr}^{cor})^S$ (red bar), as presented in Fig. 5.

The number density distributions of Z_{nr} and Z bias of two different wind speed categories are depicted in Fig. 15. The fit quadratic polynomial equation of the wind speed ≤ 6 ms^{-1} [see Fig. 15(a)] tended to descend faster than the wind speed > 12 ms^{-1} [see Fig. 15(b)], especially when $Z_{nr} > 20$ dBZ. These results revealed that a higher wind speed reduces the effect of the WRE even with larger Z_{nr} values. However, the opposite results were observed in [29]. Bechini *et al.* [29] reported a highly anisotropic attenuation caused by the rainfall above the radar, which tended to accumulate water on the upwind side of the radome, taking into account wind intensity and direction influences; they determined that the upwind have a higher Z bias than the downwind.

V. Discussion

A. Pros and Cons of the Self-Consistency Algorithm

The characteristics of K_{dp} and Z_{dr}, as well as the interdependency between Z, Z_{dr}, and K_{dp} in rain, can be used for radar calibration [17]. K_{dp} is immune to systematic bias and attenuation effect [25], and Z_{dr} reveals the mean raindrop size (e.g., mass-weighted mean diameter) of DSD [54]. However,

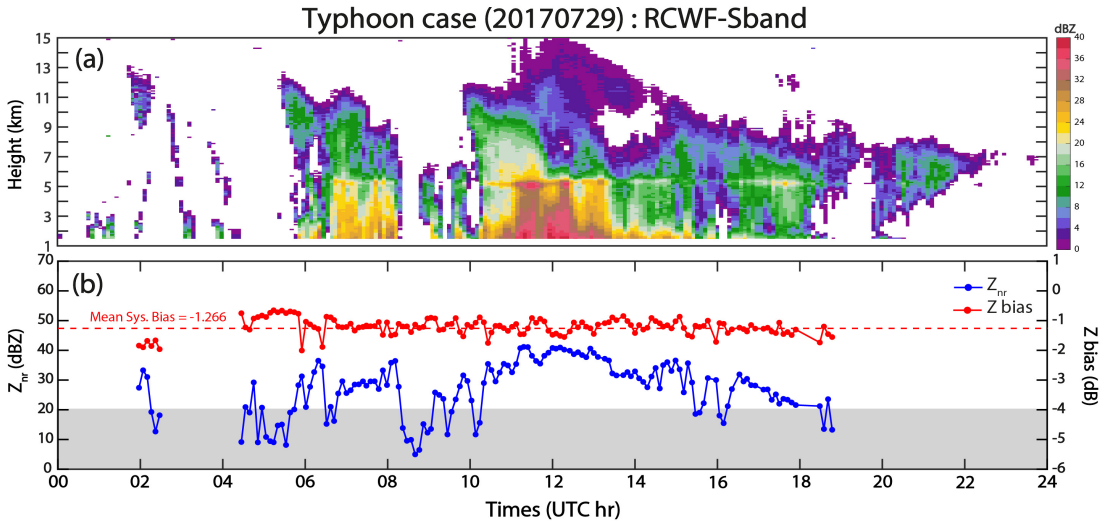

Fig. 12. Same as Fig. 10, but for the selected typhoon case (July 29, 2017) of RCWF-Sband.

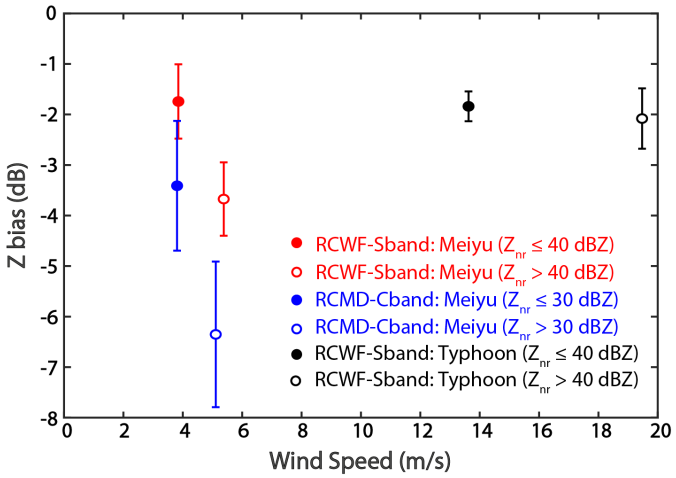

Fig. 13. Z bias with error bar, calculated using the STD, during the meiyu (blue and red) and typhoon (black) cases under different wind speeds for the following two Z ranges: ≤ 30 (blue circle) or 40 (red and black circles) and > 30 or 40 (white circles) dBZ for both radars.

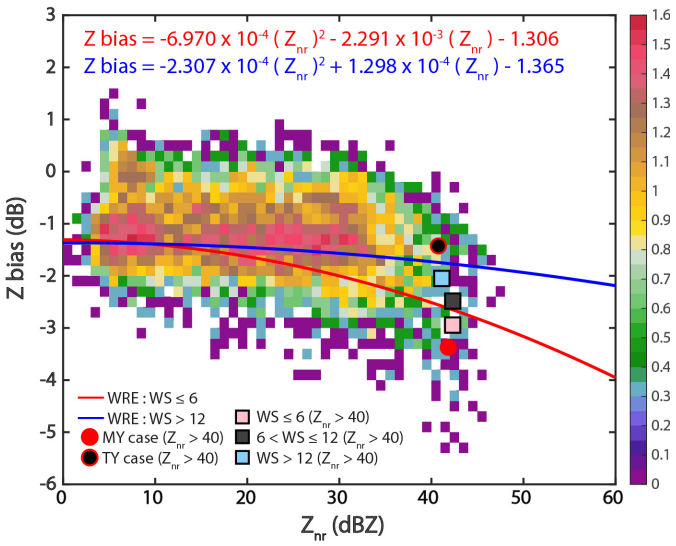

Fig. 14. Number density distribution of Z_{nr} and averaged Z bias for RCWF-Sband. The solid red and blue lines represent the Z bias in different wind speed categories: wind speed ≤ 6 ms^{-1} and wind speed > 12 ms^{-1}, respectively. The red and black circles represent the mean Z bias when Z_{nr} ≥ 40 dBZ in the meiyu and typhoon cases, respectively. The red, black, and blue squares represent the mean Z bias when Z_{nr} ≥ 40 dBZ in the three wind speed categories. WS represents the wind speed. The colorbar is in the logarithmic scale; units are counts.

the retrievals of radar variables through self-consistency relationship are subject to various uncertainties, including the assumption of the raindrop shapes (i.e., the axis ratio of a raindrop), temperature, and the DSD variability due to various microphysical processes. Ryzhkov *et al.* [17] indicated that applying spatiotemporal averaging reduces the standard error of the K_{dp} estimate substantially. Hence, comprehensive utilization of Z, Z_{dr}, and K_{dp}, thus, can estimate systematic bias with sufficient accuracy. Another uncertainty is the quality of the radar measurements; the noise and poor data quality also tend to enhance the uncertainty for radar calibration. Therefore, some procedures are needed to reduce the uncertainties caused by the DSD variabilities and radar measurements.

B. Assumptions for the Uncertainties Mitigation

In this study, only the bias caused by the transmitter and receiver chain is studied through the self-consistency relationship, which involves a few assumptions. First, it is necessary to avoid using beams with contamination from snow and ice particles since the relations used to estimate K_{dp} from Z and Z_{dr} are valid only for rain. Moreover, the quality of Z and Z_{dr} are essential to estimate the K_{dp} [see (9) and (11)]. Hence, Z^m and Z_{dr}^m must be quality-controlled from the noise and nonmeteorological (see Section II-A), unfold Φ_{dp} (see Section II-B), attenuation correction (see Section II-C), and Z_{dr} systematic bias correction (see Section II-D) before applied to the self-consistency relationship. Moreover, the raindrops are assumed to have equilibrium axis ratios, as given in [53].

The systematic bias is estimated from the $\Delta\Phi_{dp}$ and $\Delta\Phi_{dp}^e$ by self-consistency. $\Delta\Phi_{dp}$ are mostly contributed by heavy

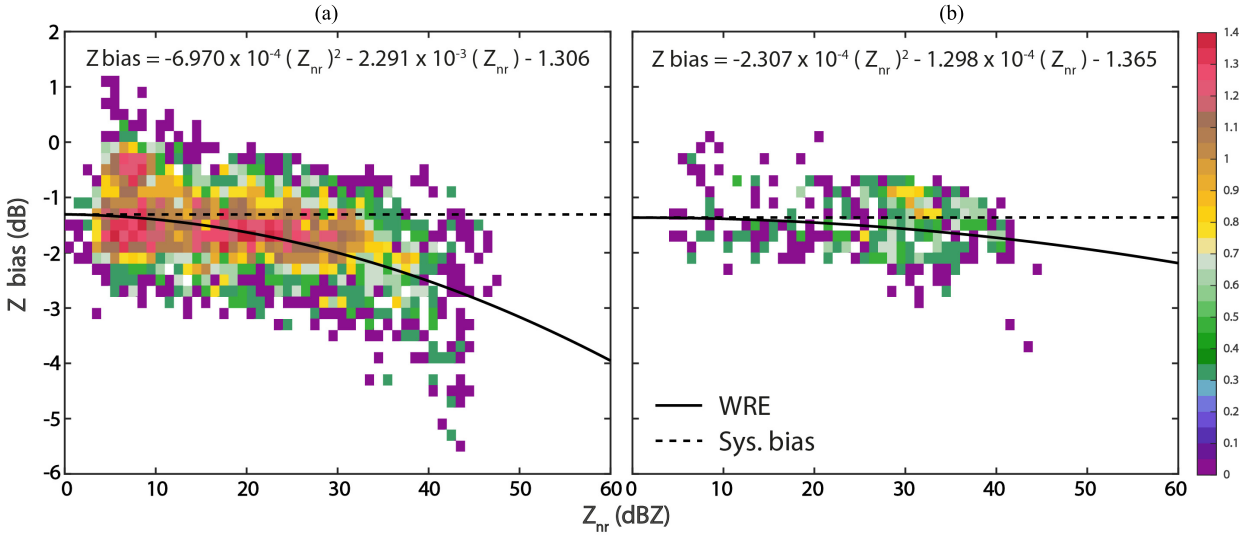

Fig. 15. Same as Fig. 14, but separated into two different wind speed categories. (a) Wind speed ≤ 6 ms^{-1}. (b) Wind speed > 12 ms^{-1}.

rain in the convection regime. The DSDs of various convection have high variability and induce uncertainty in bias estimation. The impact of DSD variability of various precipitation types (i.e., convection, stratiform, light rain, heavy rain, and so on) on self-consistency relation was mitigated by applying seasonal coefficients derived from long-term JWD data in different seasons (see Section II-F). The remaining uncertainties can be minimized in a broad statistical way, such as an average over the daily, seasonal, and annual datasets. A series of sensitivity tests were conducted to reduce the uncertainty of the self-consistency relationship. Fig. 6(c) and (d) depicts that $K_{\mathrm{dp}}(Z, Z_{\mathrm{dr}}^{\mathrm{cor}})^S$ minimizes the uncertainties of Z bias with STD values of 0.6–1.2 dB for RCWF-Sband and RCMD-Cband, respectively.

Finally, it is assumed the WRE is less sufficient when the Z_{nr} value is lower than 20 dBZ. Figs. 10–11(b) and 14 provided evidence that the Z bias has a consistent trend when Z_{nr} was lower than 20 dBZ. Hence, Z^{sys} and Z^{WRE} are adequately defined by using the threshold of Z_{nr} lower and higher than 20 dBZ, respectively.

C. Effect of WRE on Radar Data Quality

WRE has been a long-standing issue and analyzed by numerous studies (e.g., [35]–[37]). This study attempts to use radar data solely to investigate the WRE by using Z_{nr} and retrieved wind from GVAD. Certainly, additional well-coordinated rain gauge and wind measurements are helpful for operational purposes.

In this study, the Z bias of RCWF-Sband, including both systematic bias (-1.3 dB) and WRE (-1.7 dB), can reach -3 dB at approximately 48 dBZ of Z_{nr} (solid red line in Fig. 14). According to [55], S-band radar losses on hydrophobic and standard radomes can reach as much as 1 and 3 dB at R 100 mm hr^{-1}, respectively. In this meiyu case (June 1 and 2, 2017), a quasi-stationary rainband associated with the front produced hourly rainfall of 80–112 mm in northern Taiwan [56]. Hence, it is possible for RCWF-Sband radar with a semihydrophobic radome to have a loss of 1.7 dB from WRE due to heavy rainfall. Conversely, the RCMD-Cband has a higher Z bias compared to RCWF-Sband. The Z bias of RCMD-Cband also can be reached -3 dB at approximately 48 dBZ of Z_{nr} (not shown). The radome loss values of both radars were in reasonable agreement with [55]. The radome conditions, such as the material, shape, hydrophobicity of the radome coating, and surface condition, also play an important role for WRE [30], [31], [35]–[37]. It is beyond the scope of this study to investigate the aforementioned factors that require special instruments.

A significant factor, namely, wind speed, affecting the WRE was investigated in this study. As presented in Figs. 14 and 15, it is found that the WRE induced by rain atop of radar is reduced by strong wind speed. For the weak wind speed condition (i.e., less than 6 m s^{-1}), the Z bias of RCWF-Sband reached -3 dB at approximately 40 dBZ of Z_{nr}. However, the Z bias of RCWF-Sband was reduced to -2 dB given the same Z_{nr} for the strong wind speed condition (i.e., higher than 12 m s^{-1}). As [29] has illustrated that the WRE is influenced by the wind intensity and direction, the bias becomes anisotropic (azimuthal dependence) with higher winds (higher bias upwind and lower bias downwind). In this study, the impact of the wind direction on WRE was also analyzed, and the result indicates that the Z bias of RCWF-Sband was fairly consistent across the upwind and downwind directions (not shown). Further work needs to be carried out on the impact of wind direction on WRE.

Due to the location and altitude of RCMD-Cband and RCWF-Sband, as presented in Fig. 2(a), the surrounding wind of RCMD-Cband is significantly affected by the building structure of RCWF-Sband. In addition, the RCMD-Cband radar was not available during the only typhoon case in 2017 in northern Taiwan. The insufficient data of RCMD-Cband for strong wind speed study further limit the wind effect analysis. Thus, the impact of wind speed on WRE analysis was applied to RCWF-Sband radar only.

VI. Conclusion

The long-term Z bias (namely, systematic and WRE biases) of collocated operational S- and C-band dual-polarization radars was assessed in this study. Applying the attenuation, systematic bias, and WRE bias corrections reduced the errors in the Z and Z_{dr} measurements. The consistency of the corrected Z between collocated radars also considerably improved. As an innovative approach, a quadratic polynomial fitting function was proposed to explore the Z bias and Z_{nr} relations. The WRE and systematic bias can be investigated simultaneously using this quadratic polynomial equation based on different wind intensities. The products (i.e., the Z_{nr} and wind speed) obtained solely from the radar measurements were used, and the influences of precipitation atop the radome, the wind condition near the radar, and the systematic bias of Z were comprehensively investigated.

As the vertical pointing scan was not available for both radars, Z_{dr}^{sys} was estimated through statistical analysis. The results demonstrated a uniform Z_{dr}^{sys} for both radars that varied from -0.06 to 0.15 dB and -0.34 to -0.10 dB for RCWF-Sband and RCMD-Cband, respectively. Z_{dr}^{sys} of both radars was adequately small (approximately 0.2 dB variation).

The Z bias was defined as Z^{sys} when the Z_{nr} value was less than 20 dBZ, and Z^{WRE} was considered significant and, therefore, added when the Z_{nr} value was greater than 20 dBZ. Six sensitivity tests analyzed the influence of DSD variability and Z_{dr} systematic bias correction on the Z bias estimation from the self-consistency algorithm, indicating that the $K_{dp}(Z, Z_{dr})$ relation outperformed the $K_{dp}(Z)$ relation. $K_{dp}(Z, Z_{dr}^{cor})^S$ has the lowest STD and consistent Z^{sys} estimation, and thereafter, it was identified as the most suitable procedure for both radars. The seasonal mean Z^{sys} of the $K_{dp}(Z, Z_{dr}^{cor})^S$ varied from -1.89 to -1.14 dB and -2.46 to -1.87 dB for RCWF-Sband and RCMD-Cband, respectively, but, at approximately 0.6 and 1.2 dB of STD for both radars, these variabilities were adequately low.

A comparison of 940 near-synchronized volume scans from 2017 was conducted to compare the quality control improvement. All bias-corrected $Z^{Cband–Sband}$ had the highest (lowest) values of CORR (MD, STD, and RMSE) compared with the observed $Z^{Cband–Sband}$. Z^{int} of RCWF-Sband and that of RCMD-Cband were in good agreement.

The strong Z^{WRE} of a meiyu case (June 1 and 2, 2017) induced an underestimation of the reflectivity by almost 4 and 7 dB for RCWF-Sband and RCMD-Cband, respectively. The relationship between Z^{WRE} and Z_{nr} was examined using the quadratic polynomial fitting function, with the results indicating that the Z^{WRE} increases as Z_{nr} increases as a result of the accumulated rain atop the radome. However, the typhoon case (July 29, 2017) from RCWF-Sband exhibited an almost uniform Z bias, despite Z_{nr} values being higher than 30 dBZ. The influence of the wind speed on WRE was also explored, and a hypothesis was proposed that strong wind speed can reduce the WRE by removing the raindrops on the radome.

This study provided evidence that the self-consistency method allows for efficient correction of the effects introduced by the WRE and systematic biases. The stable values of the Z^{sys} of RCWF-Sband and RCMD-Cband in 2017 indicated that the CWB maintained the radar systems well. These results also indicated the influence of wind speed on the WRE. Further studies are required to gain insight into the influences of wind direction and intensity on the attenuation and WRE.

Acknowledgment

The authors would like to thank the Central Weather Bureau, Taipei, Taiwan, for providing the radar data used in this work. In particular, they thank Mike Dixon of the National Center for Atmospheric Research's Earth Observing Laboratory for his assistance with the Lidar Radar Open Software Environment.

References

[1] C.-S. Chen and Y.-L. Chen, "The rainfall characteristics of Taiwan," *Monthly Weather Rev.*, vol. 131, no. 7, pp. 1323–1341, Jul. 2003.

[2] S.-Y. Wang and T.-C. Chen, "Measuring east Asian summer monsoon rainfall contributions by different weather systems over Taiwan," *J. Appl. Meteorol. Climatol.*, vol. 47, no. 7, pp. 2068–2080, Jul. 2008.

[3] M.-T. Lee, P.-L. Lin, W.-Y. Chang, B. K. Seela, and J. Janapati, "Microphysical characteristics and types of precipitation for different seasons over north Taiwan," *J. Meteorol. Soc. Japan. II*, vol. 97, no. 4, pp. 841–865, 2019.

[4] C.-H. Tsai and C.-W. Chen, "Development of a mechanism for Typhoon- and flood-risk assessment and disaster management in the hotel industry—A case study of the hualien area," *Scandin. J. Hospitality Tourism*, vol. 11, no. 3, pp. 324–341, Oct. 2011.

[5] M.-C. Ho, D. Shaw, S. Lin, and Y.-C. Chiu, "How do disaster characteristics influence risk perception?" *Risk Anal.*, vol. 28, no. 3, pp. 635–643, Jun. 2008.

[6] L. Yang *et al.*, "A new method based on stacked auto-encoders to identify abnormal weather radar echo images," *EURASIP J. Wireless Commun. Netw.*, vol. 2020, no. 1, pp. 1–15, Dec. 2020.

[7] M. P. M. Hall, J. W. F. Goddard, and S. M. Cherry, "Identification of hydrometeors and other targets by dual-polarization radar," *Radio Sci.*, vol. 19, no. 1, pp. 132–140, Jan. 1984.

[8] P. Tabary *et al.*, "Evaluation of two 'integrated' polarimetric quantitative precipitation estimation (QPE) algorithms at C-band," *J. Hydrometeorol.*, vol. 405, nos. 3–4, pp. 248–260, 2011.

[9] J. F. I. Ventura, A.-A. Boumahmoud, B. Fradon, P. Dupuy, and P. Tabary, "Long-term monitoring of French polarimetric radar data quality and evaluation of several polarimetric quantitative precipitation estimators in ideal conditions for operational implementation at C-band," *Quart. J. Roy. Meteorol. Soc.*, vol. 138, no. 669, pp. 2212–2228, Oct. 2012.

[10] H. Liu and V. Chandrasekar, "Classification of hydrometeors based on polarimetric radar measurements: Development of fuzzy logic and neuro-fuzzy systems, and *in situ* verification," *J. Atmos. Ocean. Technol.*, vol. 17, no. 2, pp. 140–164, Feb. 2000.

[11] J.-Y. Chen, W.-Y. Chang, and P.-L. Chang, "A synthetic quantitative precipitation estimation by integrating S- and C-band dual-polarization radars over northern Taiwan," *Remote Sens.*, vol. 13, no. 1, p. 154, Jan. 2021.

[12] N. Li, Z. Wang, K. Sun, Z. Chu, L. Leng, and X. Lv, "A quality control method of ground-based weather radar data based on statistics," *IEEE Trans. Geosci. Remote Sens.*, vol. 56, no. 4, pp. 2211–2219, Apr. 2018.

[13] J. J. Gourley, A. J. Illingworth, and P. Tabary, "Absolute calibration of radar reflectivity using redundancy of the polarization observations and implied constraints on drop shapes," *J. Atmos. Ocean. Technol.*, vol. 26, no. 4, pp. 689–703, Apr. 2009.

[14] V. N. Bringi, V. Chandrasekar, N. Balakrishnan, and D. S. Zrnić, "An examination of propagation effects in rainfall on radar measurements at microwave frequencies," *J. Atmos. Ocean. Technol.*, vol. 7, no. 6, pp. 829–840, Dec. 1990.

[15] S. Kwon, G. Lee, and G. Kim, "Rainfall estimation from an operational S-band dual-polarization radar: Effect of radar calibration," *J. Meteorol. Soc. Japan. II*, vol. 93, no. 1, pp. 65–79, 2015.

[16] J. Vivekanandan, G. Zhang, S. M. Ellis, D. Rajopadhyaya, and S. K. Avery, "Radar reflectivity calibration using differential propagation phase measurement," *Radio Sci.*, vol. 38, no. 3, Jun. 2003.

[17] A. V. Ryzhkov, S. E. Giangrande, V. M. Melnikov, and T. J. Schuur, "Calibration issues of dual-polarization radar measurements," *J. Atmos. Ocean. Technol.*, vol. 22, no. 8, pp. 1138–1155, Aug. 2005.

[18] A. V. Ryzhkov and D. S. Zrnić, *Radar Polarimetry for Weather Observations*. Cham, Switzerland: Springer, 2019.
[19] W. Hitschfeld and J. Bordan, "Errors inherent in the radar measurement of rainfall at attenuating wavelengths," *J. Meteorol.*, vol. 11, no. 1, pp. 58–67, Feb. 1954.
[20] K. L. S. Gunn and T. W. R. East, "The microwave properties of precipitation particles," *Quart. J. Roy. Meteorol. Soc.*, vol. 80, no. 346, pp. 522–545, Oct. 1954.
[21] L. D. Carey, S. A. Rutledge, D. A. Ahijevych, and T. D. Keenan, "Correcting propagation effects in C-band polarimetric radar observations of tropical convection using differential propagation phase," *J. Appl. Meteorol.*, vol. 39, no. 9, pp. 1405–1433, Sep. 2000.
[22] Y.-A. Oh, D. Lee, S.-H. Jung, K.-Y. Nam, and G. Lee, "Attenuation correction effects in rainfall estimation at X-band dual-polarization radar: Evaluation with a dense rain gauge network," *Adv. Meteorol.*, vol. 2016, pp. 1–20, Jan. 2016.
[23] A. R. Jameson, "The effect of temperature on attenuation-correction schemes in rain using polarization propagation differential phase shift," *J. Appl. Meteorol.*, vol. 31, no. 9, pp. 1106–1118, Sep. 1992.
[24] W.-Y. Chang, J. Vivekanandan, and T.-C. Chen Wang, "Estimation of X-band polarimetric radar attenuation and measurement uncertainty using a variational method," *J. Appl. Meteorol. Climatol.*, vol. 53, no. 4, pp. 1099–1119, Apr. 2014.
[25] V. N. Bringi, T. D. Keenan, and V. Chandrasekar, "Correcting C-band radar reflectivity and differential reflectivity data for rain attenuation: A self-consistent method with constraints," *IEEE Trans. Geosci. Remote Sens.*, vol. 39, no. 9, pp. 1906–1915, Sep. 2001.
[26] S.-G. Park, V. N. Bringi, V. Chandrasekar, M. Maki, and K. Iwanami, "Correction of radar reflectivity and differential reflectivity for rain attenuation at X band. Part I: Theoretical and empirical basis," *J. Atmos. Ocean. Technol.*, vol. 22, pp. 1621–1632, Nov. 2005.
[27] G. Scarchilli, V. Gorgucci, V. Chandrasekar, and A. Dobaie, "Self-consistency of polarization diversity measurement of rainfall," *IEEE Trans. Geosci. Remote Sens.*, vol. 34, no. 1, pp. 22–26, Jan. 1996.
[28] E. Gorgucci and L. Baldini, "Attenuation and differential attenuation correction of C-band radar observations using a fully self-consistent methodology," *IEEE Geosci. Remote Sens. Lett.*, vol. 4, no. 2, pp. 326–330, Apr. 2007.
[29] R. Bechini, R. Cremonini, E. Gorgucci, and L. Baldini, "Dual-pol radar calibration and correction of the bias introduced by non uniform radome wetting," in *Proc. 4th Eur. Conf. Radar Meteorol. Hydrol. (ERAD)*, 2006, pp. 593–596.
[30] A. Mancini, J. L. Salazar, R. M. Lebrón, and B. L. Cheong, "A novel instrument for real-time measurement of attenuation of weather radar radome including its outer surface. Part I: The concept," *J. Atmos. Ocean. Technol.*, vol. 35, no. 5, pp. 953–973, May 2018.
[31] A. Mancini, J. L. Salazar, R. M. Lebrón, and B. L. Cheong, "A novel instrument for real-time measurement of attenuation of weather radar radome including its outer surface. Part II: Applications," *J. Atmos. Ocean. Technol.*, vol. 35, no. 5, pp. 975–991, May 2018.
[32] M. Frech, "The effect of a wet radome on dualpol data quality," in *Proc. 34th Conf. Radar Meteorol., Williamsburg, VA, Amer. Meteor. Soc. P*, vol. 13, 2009, pp. 1–7.
[33] J. L. Salazar-Cerreño *et al.*, "A drop size distribution (DSD)-based model for evaluating the performance of wet radomes for dual-polarized radars," *J. Atmos. Ocean. Technol.*, vol. 31, no. 11, pp. 2409–2430, 2014.
[34] A. Mancini, R. M. Lebron, and J. L. Salazar, "The impact of a wet S-band radome on dual-polarized phased-array radar system performance," *IEEE Trans. Antennas Propag.*, vol. 67, no. 1, pp. 207–220, Jan. 2018.
[35] M. Kurri and A. Huuskonen, "Measurements of the transmission loss of a radome at different rain intensities," *J. Atmos. Ocean. Technol.*, vol. 25, no. 9, pp. 1590–1599, Sep. 2008.
[36] E. Gorgucci, R. Bechini, L. Baldini, R. Cremonini, and V. Chandrasekar, "The influence of antenna radome on weather radar calibration and its real-time assessment," *J. Atmos. Ocean. Technol.*, vol. 30, no. 4, pp. 676–689, Apr. 2013.
[37] S. J. Frasier *et al.*, "In-place estimation of wet radome attenuation at X band," *J. Atmos. Ocean. Technol.*, vol. 30, no. 5, pp. 917–928, May 2013.
[38] J. M. Trabal, I. Zawadzki, and D. J. Mclaughlin, "A method to correct for wet radome attenuation in CASA radars by the use of a contiguous WSR-88D Radar," in *Proc. 5th Eur. Conf. Radar Meteorol. Hydrol.*, Jun./Jul. 2008.
[39] M. Schneebeli *et al.*, "Polarimetric X-band weather radar measurements in the tropics: Radome and rain attenuation correction," *Atmos. Meas. Tech. Discuss.*, vol. 5, no. 9, p. 2183, 2012.
[40] U. Germann, "Spatial continuity of precipitation, profiles of radar reflectivity and precipitation measurements in the Alps," Ph.D. dissertation, Dept. Inst. Atmos. Sci., ETH Zurich, Switzerland, 2000.
[41] A. V. Ryzhkov, S. E. Giangrande, and T. J. Schuur, "Rainfall estimation with a polarimetric prototype of WSR-88D," *J. Appl. Meteorol.*, vol. 44, pp. 502–515, Apr. 2005.
[42] L. Liu, V. N. Bringi, V. Chandrasekar, E. A. Mueller, and A. Mudukutore, "Analysis of the copolar correlation coefficient between horizontal and vertical polarizations," *J. Atmos. Ocean. Technol.*, vol. 11, no. 4, pp. 950–963, Aug. 1994.
[43] H. S. Park, A. Ryzhkov, D. Zrnic, and K.-E. Kim, "The hydrometeor classification algorithm for the polarimetric WSR-88D: Description and application to an MCS," *Weather Forecasting*, vol. 24, no. 3, pp. 730–748, 2009.
[44] R. J. Doviak and D. S. Zrnić, *Doppler Radar and Weather Observations*. New York, NY, USA: Dover, 1993.
[45] J. G. Cunningham, W. D. Zittel, R. R. Lee, R. L. Ice, and N. Hoban, "Methods for identifying systematic differential reflectivity (ZDR) biases on the operational WSR-88D network," in *Proc. 36th Conf. Radar Meteorol.*, 2013, pp. 1–24.
[46] G. W. Lee and I. Zawadzki, "Variability of drop size distributions: Time-scale dependence of the variability and its effects on rain estimation," *J. Appl. Meteorol. Climatol.*, vol. 44, no. 2, pp. 241–255, Feb. 2005.
[47] P. Tabary, G. Scialom, and U. Germann, "Real-time retrieval of the wind from aliased velocities measured by Doppler radars," *J. Atmos. Ocean. Technol.*, vol. 18, no. 6, pp. 875–882, Jun. 2001.
[48] J. Gao, K. K. Droegemeier, J. Gong, and Q. Xu, "A method for retrieving mean horizontal wind profiles from single-Doppler radar observations contaminated by aliasing," *Monthly Weather Rev.*, vol. 132, no. 6, pp. 1399–1409, Jun. 2004.
[49] M. Wang, K. Zhao, W.-C. Lee, B. J.-D. Jou, and M. Xue, "The gradient velocity track display (GrVTD) technique for retrieving tropical cyclone primary circulation from aliased velocities measured by single-Doppler radar," *J. Atmos. Ocean. Technol.*, vol. 29, no. 8, pp. 1026–1041, Aug. 2012.
[50] N. Li, M. Wei, B. Niu, J. Pan, W. Zhang, and W. Guo, "Application of multiple wind retrieval algorithms in nowcasting," *Atmosphere*, vol. 6, no. 6, pp. 834–849, Jun. 2015.
[51] B. E. Sheppard and P. I. Joe, "Comparison of raindrop size distribution measurements by a joss-waldvogel disdrometer, a PMS 2DG spectrometer, and a POSS Doppler radar," *J. Atmos. Ocean. Technol.*, vol. 11, no. 4, pp. 874–887, Aug. 1994.
[52] P.-W. Barber and C. Yeh, "Scattering of electromagnetic waves by arbitrarily shaped dielectric bodies," *Appl. Opt.*, vol. 14, no. 12, pp. 2864–2872, 1975.
[53] E. A. Brandes, G. Zhang, and J. Vivekanandan, "Experiments in rainfall estimation with a polarimetric radar in a subtropical environment," *J. Appl. Meteorol.*, vol. 41, pp. 674–685, Jun. 2002.
[54] Y. Wang, L. Tang, P.-L. Chang, and Y.-S. Tang, "Separation of convective and stratiform precipitation using polarimetric radar data with a support vector machine method," *Atmos. Meas. Techn.*, vol. 14, no. 1, pp. 185–197, Jan. 2021.
[55] F. J. Merceret and J. G. Ward, "Attenuation of weather radar signals due to wetting of the radome by rainwater or incomplete filling of the beam volume," NASA Tech. Memo., NASA Kennedy Space Center, FL, USA, Tech. Rep. NASA/TM-2002-211171, 2002, vol. 16.
[56] C.-C. Wang, M.-S. Li, C.-S. Chang, P.-Y. Chuang, S.-H. Chen, and K. Tsuboki, "Ensemble-based sensitivity analysis and predictability of an extreme rainfall event over northern Taiwan in the Mei-Yu season: The 2 June 2017 case," *Atmos. Res.*, vol. 259, Sep. 2021, Art. no. 105684.

Jui Le Loh received the B.S. degree in oceanography and the M.S. degree in climatology from the National University of Malaysia, Bangi, Malaysia, in 2009 and 2013, respectively, and the Ph.D. degree in radar meteorology from Pukyong National University, Busan, South Korea, in 2017.

She is a Post-Doctoral Researcher with the Department of Atmospheric Sciences, National Central University, Taoyuan, Taiwan. Her research interests include cloud and precipitation microphysics, radar data quality control, meteorological applications of polarimetric radar, and climate variability and change in Malaysia.

Wei-Yu Chang received the bachelor's degree in atmospheric sciences from the Chinese Culture University, Taipei, Taiwan, in 2000, and the M.S. and Ph.D. degrees in atmospheric sciences from the National Central University (NCU), Taoyuan, Taiwan, in 2002 and 2010, respectively.

He was a Post-Doctoral Fellow with the Advanced Study Program (ASP), Earth Observing Laboratory (EOL), National Center for Atmospheric Research (NCAR), Boulder, CO, USA, from 2011 to 2014. He was an Assistant Professor with the Chinese Culture University from 2015 to 2019. Since 2020, he has been an Assistant Professor at NCU. His research interest includes mainly advancing the understanding of the precipitation processes of mesoscale convective systems using meteorological radar. He also specializes in various radar data techniques, including raindrop size distribution retrieval, quantitative precipitation estimation (QPE), hydrometer classification, storm tracking, non-meteorological signal removal, and attenuation correction.

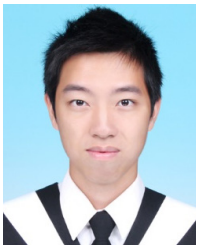

Hsiu-Wei Hsu received the B.S. and M.S. degrees in atmospheric sciences from the National Central University, Taoyuan, Taiwan, in 2017 and 2019, respectively.

He is a Research Assistant with the National Central University, where he is in charge of the improvement of data quality and the development of particle identification techniques. His research interests include signal processing to capture the detailed information from the Doppler spectrum to investigate the physical mechanism of extreme weather and radar refractivity to understand the interaction between near-surface water moisture fields and the various weather systems.

Pin-Fang Lin received the bachelor's degree in atmosphere science from the Chinese Cultural University, Taipei, Taiwan, in 2000, and the M.S. and Ph.D. degrees in atmosphere science from the National Taiwan University (NTU), Taipei, in 2002 and 2011, respectively.

She is currently a Senior Technical Section Chief with the Central Weather Bureau (CWB), Taipei. Her research interests include radar data application, including quantitative precipitation estimation (QPE), data quality improvements, and so on.

Pao-Liang Chang received the bachelor's degree in atmosphere science from the Chinese Culture University, Taipei, Taiwan, in 1990, and the M.S. and Ph.D. degrees in atmosphere science from the National Taiwan University (NTU), Taipei, in 1993 and 2000, respectively.

He is a Senior Technical Specialist with the Central Weather Bureau (CWB), Taipei, Taiwan. His first position in 1995 was the Radar Meteorologist at the Wu-Fen-San radar site, where the first Doppler radar (WSR-88D) of CWB was installed. Since 2003, he has directed the development of the CWB radar operation system in collaboration with the National Severe Storms Laboratory (NSSL), Norman, OK, USA. In 2011, he was promoted to be the Section Chief to manage the operation and maintenance of the CWB Doppler radar network. In 2018, his new position was in charge of the development of operational numerical weather prediction systems, including radar data assimilation systems. During his career in CWB, he dedicated himself to operational technical developments and shared his research experiences.

Dr. Chang also serves as an Associate Editor for *Journal of Applied Meteorology and Climatology*.

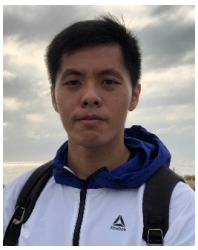

Yung-Lin Teng received the B.S. degree in industrial engineering and management from the National Chiao Tung University, Hsinchu, Taiwan, in 2013, and the M.S. degree in atmospheric sciences from the National Central University, Taoyuan, Taiwan, in 2015.

He is working with the Department of Atmospheric Sciences, National Central University. His research activities include wind synthesis and thermodynamic retrieval in radar meteorology applications.

Yu-Chieng Liou received the bachelor's degree from the National Taiwan University, Taipei, Taiwan, in 1983, and the M.S. and Ph.D. degrees from the School of Meteorology, University of Oklahoma, Norman, OK, USA, in 1989 and 1995, respectively.

He is a Distinguished Professor with the Department of Atmospheric Sciences, National Central University (NCU), Taoyuan, Taiwan. His research interests include radar meteorology, data retrieval and assimilation, rainfall mechanisms, and short-term quantitative precipitation forecast.

Dr. Liou was the project PI to build the very first X-band dual-pol mobile weather radar in Taiwan. He has served as the Department Chair, the Deputy Director General of Taiwan Typhoon and Flood Research Institute, and the Director of Earth Science Research Promotion Center under the Ministry of Science and Technology (MOST) of Taiwan. He received the Outstanding Research Award from NCU, the Future Tech Award from MOST, and the Korea Government Award. He is the Chairperson of the Project Review Committee under MOST and an Associate Editor of *Monthly Weather Review*.